Modeling Conformational Dynamics of Cisplatin and Oxaliplatin Adducts with DNA

Peng Gong

A thesis submitted to the faculty of the University of North Carolina at Chapel Hill in partial fulfillment of the requirements for the degree of Master of Science in the Department of Biomedical Engineering.

Chapel Hill

2006

Approved by,

Professor Stephen G. Chaney
Professor Henry S. Hsiao
Professor Carol N. Lucas

ABSTRACT

Peng Gong: Utilizing Molecular Dynamics to Study Conformation and Conformational Dynamics of Cisplatin and Oxaliplatin Adducts with DNA

(Under the direction of Stephen G. Chaney)

Cis-diamminedichloroplatinum(II) (cisplatin, CP) is a widely used anti-cancer agent. Its platinum analog (*trans*-R,R)1,2-diaminocyclohexaneoxalatoplatinum(II) (oxaliplatin, OX) is often effective in cisplatin resistant tumors and generally causes less mutation than CP. Although their carrier ligands are structurally distinct, CP and OX form the same types of adducts at the same sites on the DNA. Certain DNA regulatory proteins could distinguish CP-DNA adducts from OX-DNA adducts but the underlying mechanism is not clear currently. In this thesis, we utilized molecular dynamics computer simulation to study these two adducts and we found that DNA was more distorted on the 5' side of the adduct than the 3' side, CP adduct was oriented more towards the 5' side of the adduct and OX adduct more towards the 3' side and some significant differences were observed in the frequency distributions of DNA duplex helical parameters, which may provide an explanation to their distinct biological properties.

To my wife Yixing Zhou, my parents Hongbin Hu and Benzhi Gong, and my parents in law, Fengzhen Zhang and Yuehan Zhou, who always support and encourage me.

ACKNOWLEDGEMENTS

The author would like to thank Dr. Stephen G. Chaney for providing knowledge and financial support, especially the valuable opportunity for me to study in this area; Dr. Feng Ding, current and previous members from Dr. Nikolay V. Dokholyan's lab for helpful advice on molecular dynamics simulations and trajectory analysis; Dr. Debadeep Bhattacharyya, current and previous members from Dr. Stephen G. Chaney's lab and Dr. Yibin Wu for helpful discussion on NMR solution structures; Dr. Brenda R. S. Temple for help in every aspect of this work; the ITS (Information Technology Service) Department at UNC for providing the computer clusters, Gaussian 03, AMBER v8.0 and other various software packages and technique support; Dr. Henry S. Hsiao and Dr. Carol N. Lucas from my home department for spending time on advising me and reading my thesis; my home department Biomedical Engineering for giving me such a wonderful opportunity to study here for the past five years. This work is supported by NIH grant CA84480.

TABLE OF CONTENTS

LIST OF TABLES

LIST OF FIGURES

LIST OF ABBREVIATIONS

CP cisplatin

CRY crystallography

MD molecular dynamics

NMR nuclear magnetic resonance

OX oxaliplatin

LIST OF SYMBOLS

Å **angstrom**

º **degree**

CHAPTER 1 BACKGROUND

1.1 Cisplatin is a potent platinum agent in chemotherapy against cancers

Cisplatin (CP) or *cis*-diamminedichloroplatinum(II) (CDDP) is a platinum-based drug used in chemotherapy to treat cancers, such as testicular, ovarian, bladder, gullet (oesophagus), stomach, head, neck and non-small cell lung cancer.

1.1.1 Chemical structure of cisplatin

Cisplatin is a surprisingly simple inorganic compound and its chemical structure in 2D and 3D is shown in Figure 1.1. Cisplatin has a square-planar structure, with central platinum (Pt) coordinated by two chloride (Cl) ion ligands *cis* to each other and other two ammonia (NH_3) ligands also in *cis*.

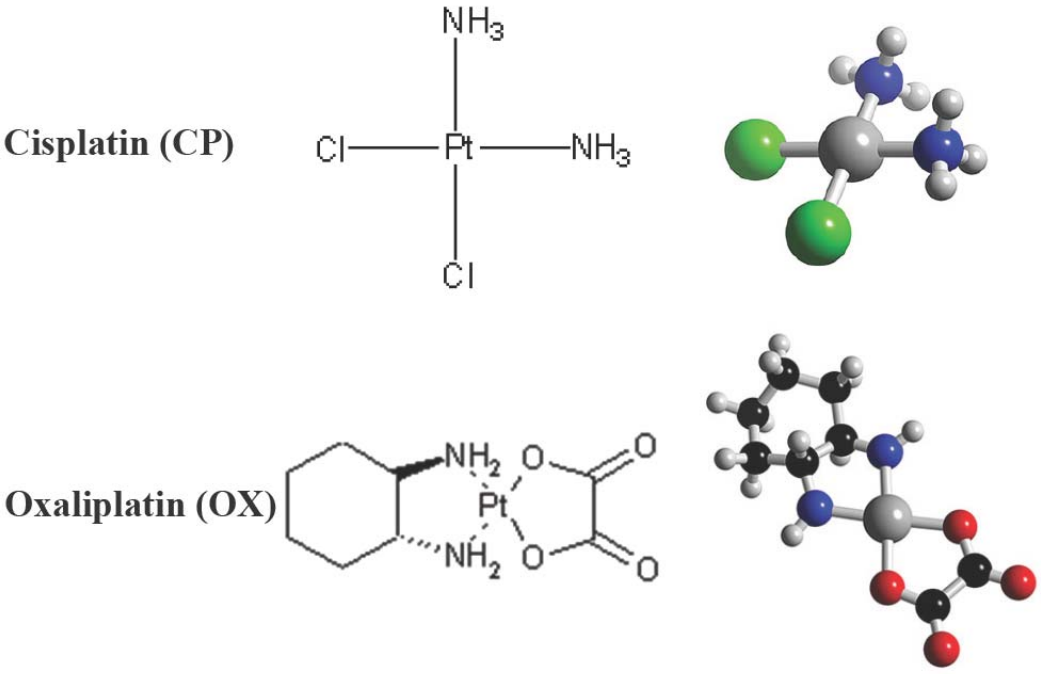

Figure 1.1 The chemical structures of cisplatin and oxaliplatin in 2D and 3D. The upper panel is the chemical structure of cisplatin in 2D and 3D, the central platinum atom in big gray ball, chloride in green, nitrogen in blue and hydrogen in small gray ball. The lower panel is the chemical structure of oxaliplatin in 2D and 3D, the central platinum atom in big gray ball, oxygen in red, nitrogen in blue, carbon in black and hydrogen in small gray ball.

1.1.2 History of discovery of cisplatin

Cisplatin is a chemical compound discovered in 1844 and was only found to have anticancer properties in 1970s by accident. As a chemical compound, cisplatin was first synthesized by M. Peyrone in 1844 and had been called Peyrone's chloride. Its chemical structure was first elucidated by Alfred Werner in 1893. In the early 1960s cisplatin was rediscovered by Barnett Rosenberg *et. al.* at Michigan State University in a series of experiments designed to elucidate the effect of electric fields on the bacterial growth of *E. coli*. What they observed was that the bacteria grew into an elongated form, 300 times the normal length, and unexpectedly, ceased to divide. After careful examination a year later the cause of inhibition of bacteria division was shown not to be due to the electric fields but rather a platinum compound formed in a reaction between the platinum electrodes and components of the solution. Further tests revealed that this platinum compound could prevent cell divisions through inhibition of cell mitosis, but not other growth processes in the bacteria, resulting in bacteria elongation. This serendipitous discovery soon initiated a series of investigations and studies into the effects of platinum compounds on cell division. In 1970, further studies by Barnett Rosenberg revealed that some platinum compounds had significant anticancer activity and demonstrated that diamminedichloroplatinum(II), specifically the *cis* isomer cisplatin, was extremely effective against sarcoma 180 and L1210 leukemia in mice. Cisplatin was the first member of its class to be approved for clinical use by the American Food and Drug Administration (FDA) in 1978. Cisplatin has been one of the most effective, widely used and most profitable antineoplastics in the world.

1.1.3 Mechanism of cisplatin against tumors

The clinical efficacy of cisplatin in chemotherapy against tumors is thought to be primarily due to the formation of cisplatin-DNA adducts which interfere with cellular repair and replication, and therefore trigger a chain of cell regulatory events, ultimately leading to cell death.

The details of formation of cisplatin-DNA adducts are as follows. The uncharged cisplatin is able to cross the cell membrane and enter the cell. The relatively low concentration of chloride in cytosol favors the substitution of chloride ions with water molecules. This results in positively charged, active, aquated species, which can be easily attacked by a variety of macromolecules possessing nucleophilic groups, including DNA. While platinum adducts with protein and RNA are more abundant, the Pt-DNA adducts are thought to be responsible for killing the cell. Cisplatin can form coordinated covalent bonds with

nucleophilic sites on nucleic acid bases in DNA. Its preferential binding sites are the N7 atom of guanine base especially in regions of two or more consecutive guanines, and to a lesser extent, the N7 atom of adenine base when it is located 5' to a guanine([4]) (Figure 1.2). Generally speaking, cisplatin is a bifunctional agent and can bind to two sites in DNA. The resulting biadducts are composed of approximately 60-65% 1,2-intrastrand GG, 25-30% 1,2-intrastrand AG, 5-10% 1,3-intrastrand GNG and 1-3% interstrand GG([1]) (Figure 1.2).

1.1.4 Side effects and limitations of cisplatin

Cisplatin is cytotoxic and has severe toxic side effects in clinical practices, such as nephrotoxicity, neurotoxicity, ototoxicity, extremely severe nausea and vomiting, and other toxic manifestations common among anticancer agents. In addition, although the mutagenicity of cisplatin has not been officially determined or acknowledged, the International Agency for Research on Cancer (IARC) has classified cisplatin as a probable human carcinogen([2]). Furthermore, acquired resistance can develop against cisplatin in some types of tumors during the treatment process, which reduces the clinical efficacy of cisplatin. All of the above side effects and limitations of cisplatin have promoted research and development of second generation platinum agents, which are designed to have greater clinical effectiveness, reduced cytotoxicity and modified, more "friendly" pharmacological properties. Oxaliplatin is such a successful successor.

1.2 Oxaliplatin is the second generation platinum analog of cisplatin

Studies have shown that even minor variation of the carrier ligands of platinum complex could possibly have a profound effect on its anticancer activity and cytotoxicity. For example, almost all *trans*-compounds tested are ineffective, while the *cis*-counterparts are quite the opposite. After screening hundreds of platinum complexes, there are only a few successful ones, of which one is oxaliplatin (OX) or (*trans*-R,R)1,2-diaminocyclohexaneoxalatoplatinum(II). Oxaliplatin is a much bigger organic compound and its chemical structure in 2D and 3D is shown in Figure 1.1. Compared to cisplatin, the two amine NH_3 ligands in cisplatin are substituted by the (*trans*-R,R)1,2-diaminocyclohexane (DACH) ligand in oxaliplatin in order to improve antitumour activity; the two chloride ion ligands in cisplatin are replaced by the oxalato bidentate ligand derived from oxalic acid in oxaliplatin in order to improve water solubility. Although structurally distinct from each other, studies have shown that cisplatin and oxaliplatin form the same types of adducts at the same sites in DNA([5]). Cisplatin forms cisplatin-DNA adduct with *cis*-diammine carrier

ligand and oxaliplatin forms oxaliplatin-DNA adduct with much bulkier DACH carrier ligand (Figure 1.2). However, oxaliplatin is generally more effective in certain cisplatin-resistant cell lines([3]) and the FDA approved its clinical usage for the treatment of colorectal cancer and other cisplatin-resistant tumors in 2004. Oxaliplatin has become the third most widely used platinum agent in the world for treatment of cancer.

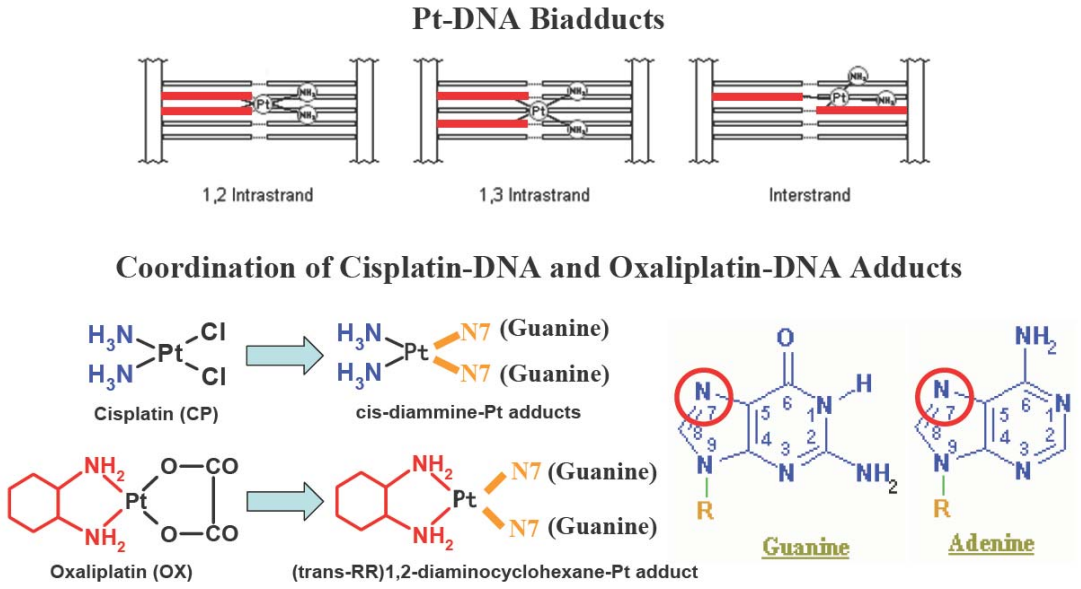

Figure 1.2 Formation of cisplatin-DNA and oxaliplatin-DNA adducts. The upper panel shows the three major kinds of Pt-DNA biadducts. The red bar represents the nucleotide which is coordinated by the platinum adduct. The lower panel illustrates how the two chloride ion ligands of cisplatin and the oxalato bidentate ligand of oxaliplatin are substituted by the N7 atom from two guanines or one adenine.

1.3 Research on cisplatin and oxaliplatin

The elucidation of the molecular basis of the reduced mutagenicity and enhanced cytotoxicity of oxaliplatin in cisplatin-resistant tumors would make a significant contribution to the development of the third generation platinum drugs with greater efficacy and less toxicity. Extensive research and studies on cisplatin, oxaliplatin and their DNA adducts have been carried out. Recent interest has been focused on the interactions between their DNA adducts and cellular regulatory proteins vital for cellular repair and replication.

1.3.1 Research methods

Besides the *in vivo* and *in vitro* experiments, the study on molecular structure is another important direction. Only a few experimental structures of cisplatin-DNA or oxaliplatin-DNA adducts are currently available in the Research Collaboratory for Structural Bioinformatics (RCSB) data bank on line. These experimental structures have been solved either by x-ray crystallography or by nuclear magnetic resonance

(NMR) in various conditions. Reproducing these structures or comparing results is difficult.

Molecular dynamics (MD) simulation is a special discipline of molecular modeling. One of its applications is actually used as an important tool in crystallography and NMR for structural determination and refinement. However, more significantly, just as its name implies, MD can be used to provide "dynamic" information, in other words, time-dependent properties of molecular system, which is not available from experimental structures. Therefore, in this thesis work, we decided to utilize molecular dynamics simulation to facilitate our study on cisplatin-DNA and oxaliplatin-DNA adducts.

1.4 Molecular dynamics simulation

Molecular dynamics computer simulation is most commonly used to simulate the dynamics of known structures. Conformational transitions and local vibrations are the usual subject of molecular dynamics studies.

Molecular dynamics largely relies on numerically solving Newton's equations of motion on an atomistic model of a molecular system to obtain the positions of each atom along a series of extremely small time steps in the order of femtoseconds (10^{-15}). The resulting series of snapshots of molecular motion dynamics over time is called a simulation trajectory. Energy and other intermediate calculation results can be recorded along with the trajectory. Time-dependent properties and other valuable information can thus be derived from the trajectory. The initial coordinates of the molecular system generally come from the experimental structures and/or molecular modeling. The initial velocity of each atom is assigned randomly but normally following a Maxwell distribution. The velocities have to conform to the total kinetic energy of the system, which in turn, is dictated by the desired simulation temperature. It is achieved by slowly heating the system and then allowing the energy to equilibrate among the atoms. The details of how the position of an atom at the next time step is calculated from its current position and velocity are as follows. First, the energy has to be calculated using either classical mechanics or quantum mechanics methods. Classical mechanics are generally employed but limited to applications that do not involve drastic changes such as bond making or breaking. Quantum mechanics can be applied to study of dynamic processes involving chemical reactions but the energy calculation can be extremely difficult and time-consuming. Once the energy and current position are known, the forces can be calculated as the derivative of the energy with

respect to the change in position. With the derived force and known mass of the atom, the acceleration, velocity and position can be calculated sequentially. In detail, for example, the "leapfrog" algorithm, shown in Figure 1.3 is commonly used to numerically integrate Newton's second law in molecular dynamics simulations. For atom i at time t, time step Δt, velocity v and position r are successively updated every half of the time step.

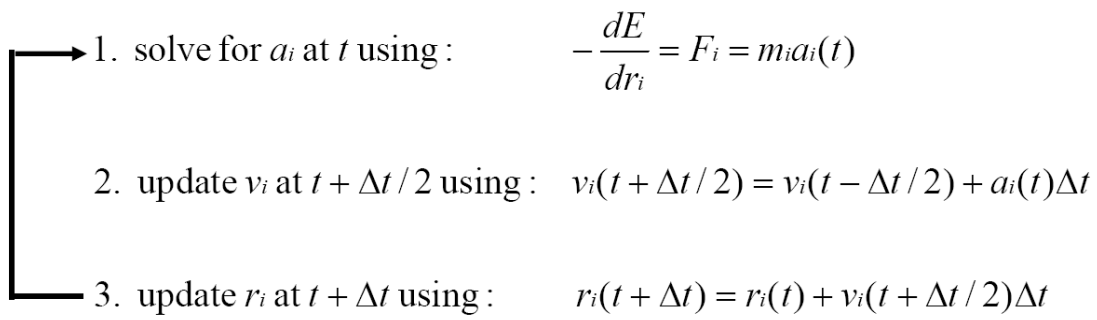

Figure 1.3 The Scheme of "Leapfrog" Algorithm.

Another fundamental part of molecular dynamics is the so called force field. A force field refers to a group of equations and parameter sets used to describe the interactions among atoms within a molecular system. A force field can be empirical, semi-empirical or derived from quantum mechanics.

Molecular dynamics does have its own limitations as well. As mentioned earlier, it is almost unfeasible to simulate dynamic processes involving chemical reactions. Besides theories and methods which are still far from perfection, the applications of molecular dynamics are often restricted by current computational power. The size of molecular system and length of simulation time must be designed carefully so that the calculation can finish within a useful time period, which restraints studies on multi- and macro- molecular systems and in a long and more physiologically relevant time scale.

We decided to use AMBER (Assisted Model Building and Energy Refinement) software for our molecular dynamics simulations because AMBER is widely used for proteins and DNA. However, the force field parameters for Pt-GG adducts are not defined in AMBER and the currently available force field parameters for Pt-GG adducts are not robustly determined due to limitations in techniques and computational power of the time. Therefore we decided to recalculate the atomic partial charges of Pt-GG adducts using *ab-initio* method, which fully relies on quantum mechanics. Other force field parameters for

Pt-GG adducts were inherited from previous work.

1.5 Thesis outline

In chapter 2, I will describe my work on a comparison study of cisplatin-DNA and oxaliplatin-DNA adducts utilizing molecular dynamics simulation. Chapter 3 includes a general discussion and suggestions for future directions.

REFERENCES

1. Eastman, A. (1987). The formation, isolation and characterization of DNA adducts produced by anticancer platinum complexes. *Pharmacol. Ther.* **34**, 155-166.

2. International Agency for Research on Cancer. Overall Evaluations of Carcinogenicity: An updating of *IARC Monographs* volumes 1 to 42. [Supplement 7]. 1987. Lyon, France, World Health Organization. International Agency for Research on Cancer.

3. Kidani, Y. (1989). Oxaliplatin. *Drugs of the Future* **14**, 529-532.

4. Mansy, S., Rosenberg, B., & Thomson, A. J. (1973). Binding of cis- and trans-dichlorodiammineplatinum(II) to nucleosides. I. Location of the binding sites. *J. Am. Chem. Soc.* **95**, 1633-1640.

5. Page, J. D., Husain, I., Sancar, A., & Chaney, S. G. (1990). Effect of the diaminocyclohexane carrier ligand on platinum adduct formation, repair, and lethality. *Biochemistry* **29**, 1016-1024.

CHAPTER 2 THESIS WORK

2.1 Introduction

Since 1978, *cis*-diamminedichloroplatinum(II) (cisplatin, CP) has been the most widely used platinum (Pt) agent in chemotherapy as a treatment for certain cancers, such as testicular, ovarian, bladder, gullet (oesophagus), stomach, head, neck and non-small cell lung cancer. However, besides severe clinical side effects, such as nephrotoxicity and ototoxicity, the major limitations of CP are its cytotoxicity, mutagenicity, and the intrinsic or acquired resistance to CP in certain tumors. As a cisplatin analog, (*trans*-R,R)1,2-diaminocyclohexaneoxalatoplatinum(II) (oxaliplatin, OX) is the third most widely used platinum agent in chemotherapy. The FDA recently approved OX for the treatment of colorectal cancer and CP-resistant tumors. The clinical efficacy of CP and OX toward cancer cells is thought to result primarily from the formation of Pt-DNA adducts which prevent DNA replication and trigger a series of cell regulatory events that ultimately lead to cell death. We([13]) and others([6,18]) have found that CP and OX form the same types of adducts at the same sites on the DNA, although CP forms CP-DNA adducts with *cis*-diammine carrier ligand and OX forms OX-DNA adducts with (*trans*-R,R)1,2-diaminocyclohexane (DACH) carrier ligand. The major Pt-DNA adducts form as intrastrand-GG adducts which account for 60-65%. OX-DNA adducts have been reported to be less mutagenic in Ames test with *S. typhimurium*([7,9]) and in human cell lines than CP-DNA adducts. The apparent clinical differences between CP and OX in their cytotoxicity, mutagenicity and efficacy in tumors are thought to be due to the differential recognition of CP-DNA and OX-DNA adducts by proteins involved in DNA damage-recognition and repair mechanisms. For example, some DNA damage-recognition proteins, especially those of the HMG-domain family, bind more tightly to CP-DNA adducts than to OX-DNA adducts([17,23]); the DNA mismatch repair complexes hMSH2([5]) and MutS([22]) bind with greater affinity to CP-DNA adducts than to OX-DNA adducts; the DNA polymerases η and β both catalyze translesion synthesis bypassing OX-DNA adducts with higher efficiency than CP-DNA adducts([3]). Here we hypothesize that the differential recognition of CP-DNA and OX-DNA adducts by a wide range of proteins involved in DNA damage-recognition and repair is due to the differences in conformation and/or conformational dynamics between CP-DNA and OX-DNA adducts.

The crystal structures of CP-DNA and OX-DNA adducts in the same dodecamer DNA sequence have been reported. The two structures were very similar except for the nature of the carrier ligand in the major groove and two potential hydrogen bonds between ligand and DNA. One hydrogen bond was reported to be between 5' ammine NH_3 ligand and the terminal oxygen atom of 5' G* (the guanine coordinated to the platinum adduct) phosphate group in CP-DNA adduct([16]). The other was between 3' amine NH_2 group of DACH ligand and the O6 atom of 3' G* in OX-DNA adduct([15]). There exist conformational differences between CP-DNA and OX-DNA adducts. However, the possible differences in their conformational dynamics have not been elucidated in previous studies. In addition, although considerable differences between Pt-DNA adducts and undamaged DNA have been reported, no previous studies have compared them under the same conditions in the same DNA sequence context. Here, in this study, we used molecular dynamics (MD) simulation to explore the differences in conformation and conformational dynamics between CP-DNA and OX-DNA adducts, and between Pt-DNA adducts and undamaged DNA, using the same DNA sequence context.

The previously available atomic partial charges of CP-GG and OX-GG adducts were not rigorously determined due to the limitations of knowledge and computational power at the time. Therefore we recalculated these charges using well-accepted methods and the most updated quantum mechanics program Gaussian03. All the other force field parameters of CP-GG and OX-GG adducts were referenced, extended or modified based on AMBER parm99 force field parameters and previous work by Yao *et al.*([21]), Scheeff *et al*([14]). and Kozelka *et al*([4]). The simulation protocol had been refined for Pt-DNA adducts. Altogether we did twenty-five 10 ns unrestrained and fully solvated MD simulations using AMBER v8.0. All twenty-five simulations reached equilibrium within 2 ns and therefore, the structures in the final 8 ns were used for conformation and conformational dynamics analysis. The equilibrium structures were independent of the initial conditions and were in good agreement with the NMR data. The geometry of Pt-GG adducts was intuitively reasonable. Our data derived from MD simulation trajectories showed greater distortion at the 5' G* of both CP-GG and OX-GG adducts in agreement with previous NMR structures and MD simulation studies. Our data suggested that the differences between the 5' and 3' G* of Pt-GG addcuts might be due to the different flexibility of the phosphodiester bond connecting the 5' and 3' G*. Our data also showed several differences between CP-DNA and OX-DNA adducts, including the preferential orientation of the

platinum carrier ligand to the 5' or 3' side of the adduct and the frequency distributions of several DNA duplex helical parameters of the central four base pairs surrounding the platinum adduct. The differences in conformation and conformational dynamics may provide a biological explanation to the discrimination between CP-DNA and OX-DNA adducts by those specific DNA proteins. We postulate that CP-DNA adducts may adopt favorable conformations for binding DNA damage-recognition proteins, such as HMG-domain proteins and DNA mismatch repair complex more frequently than OX-DNA adducts; however, as for DNA polymerases η and β, it may be the other way around. Future NMR and MD studies are planned to test this hypothesis.

2.2 Method

2.2.1 Starting structures

All five starting structures contained 12-mer DNA duplex in the same sequence context 5'-d(CCTCAG*G*CCTCC)-3'. The NMR solution structures of CP-DNA adduct (data not published), OX-DNA adduct (1PGC.pdb([19])) and undamaged B-form DNA (B-DNA, data not published) solved in our lab were used as three starting structures. The other two starting structures were derived from the NMR solution structure of hSRYHMG complexed to DNA (1J46.pdb([12])) for the DNA backbone, the x-ray crystallography structure of CP·DNA·HMG complex (1KSB.pdb([10])) for the CP-GG adduct and our NMR solution structure of OX-DNA (1PGC.pdb) for the OX-GG adduct. In the molecular modeling program, we manually built these two starting structures, one CP-DNA adduct and one OX-DNA adduct, using insightII (Molecular Simulations Inc., San Diego). The original DNA sequence from 1J46.pdb was mutated to the same DNA sequence used for our NMR solution structures. The templating DNA backbone, which was more bent than the DNA in the NMR solution structures, provided a good test of whether our MD simulations were capable of driving very different starting structures to non-distinguishable structures when simulations reached equilibrium.

2.2.2 Force field parameterization

The force field parameters, including the atomic partial charges for CP-GG and OX-GG adducts are not defined in the standard AMBER force field library. However, they are required and crucial in MD simulations. In order to determine the atomic partial charges of CP-GG and OX-GG adducts, the

9-methyl-guanine derivatives *cis*-$[Pt(NH_3)_2(9\text{-Me-Guo})_2]^{2+}$ (CP-meG$_2$) and $[Pt(DACH)(9\text{-Me-Guo})_2]^{2+}$ (OX-meG$_2$) were used to simplify the calculation. These derivatives were manually built from our NMR solution structures by using insightII. Gaussian03 was employed to quantum mechanically optimize the geometry of these derivatives and to determine the partial charge on each atom. Density functional method B3LYP implemented within Gaussian03 was utilized; LanL2DZ basis set was used exclusively for the platinum atom and 6-31Gd basis set was used for the rest of the atoms. The atomic partial charges were determined using Mulliken method implemented within Gaussian03 based on either the structure geometry optimized by Gaussian03 or the NMR structure modified to the 9-methyl-guanine derivative. The Mulliken method turned out to be insensitive to the geometry of the structure and the resulting atomic partial charges were consistent in every geometry optimized or non-optimized structure. The partial charge of the platinum atom was close to the previously published value, while the partial charges of four nitrogen atoms surrounding the platinum atom were significantly different from the previously published values. The partial charges of the rest of the atoms were within the theoretical range and comparable with their counterparts in the standard force filed. The Mulliken charges based on the structure of the original 9-methyl-guanine derivative modified from our NMR solution structure without further geometry optimization were used as the new atomic partial charges for Pt-GG adducts and incorporated into our force field parameters. The atomic partial charges of chemically equivalent atoms (such as the pseudo-equatorial hydrogen atoms of the ammine group, the corresponding atoms in the two guanine bases etc.) were averaged and the small charge discrepancy due to the structural difference between 9-methyl-guanine and deoxyguanine was distributed to the sugar according to the standard charge transfer technique used by Yao *et al.*([21]). Besides the atomic partial charges, other force field parameters of Pt-GG adducts were referenced from AMBER parm99 force field parameters or from previous work by Yao *et al.*([21]) and Scheeff *et al.*([14]).

2.2.3 MD simulation protocol

The starting structures described earlier were first modified by removal of hydrogen atoms in insightII and were further prepared by LEaP module of AMBER v8.0. The Cornell *et al*. force field and parm99 parameter set were used, as well as our self-defined force field parameters for Pt-GG adducts. The Generalized Born parameters were set to use modified Bondi radii (where the radius of hydrogen bonded to oxygen or sulfur was set to 0.8 Å; hydrogen bonded to carbon was 1.3 Å; hydrogen bonded to nitrogen was 1.3 Å). The procedures for preparing structures for MD were as following. Firstly hydrogen atoms were

added back according to the nucleotide templates in AMBER force field library "all_nucleic94.lib". Secondly the structures were neutralized with counter-ions. 19, 20 and 22 sodium ions Na^+ were added and placed by LEaP to the system of CP-DNA, OX-DNA and B-DNA respectively. Thirdly the neutralized system was fully solvated in a rectangular parallelepiped water box using default TIP3 model water molecules. The distance between the wall of the periodic box and the closest atom in the solute was set to be 12.5 Å. There were 7495, 7264 and 6957 water molecules added to the system of CP-DNA, OX-DNA and B-DNA respectively. This yielded a periodic cubic box with edge approximate 70 Å for the three systems.

The whole system underwent 120 ps minimization and relaxation before a 10 ns production MD carried out by SANDER module of AMBER v8.0. The nonbonded cutoff was set to be 9.0 Å and the nonbonded list was updated every 10 steps. No Generalized Born term was used. The MD simulations were always carried out in NPT condition (constant pressure, using isotropic position scaling, at 1 atm (1 atm = 6.9 kPa), pressure relaxation time constant 0.2 ps in relaxation MD and 2 ps in production MD; constant temperature, using weak-coupling algorithm, at 300 K, heat bath coupling time constant 0.2 ps in relaxation MD and 1 ps in production MD) with a 1 fs time step. In MD simulations, the SHAKE algorithm was applied to all bonds involving hydrogen atom and in turn the regular force evaluation omitted those bonds. The translational center-of-mass motion was removed every 1 ps. Every time the system was heated up, zero velocity information was inherited from the previous stage and a Maxwell distribution of velocities was re-established. In minimization and relaxation, a harmonic potential was applied to Pt-DNA adduct or DNA to restrain its motion. The restraint was gradually weakening and became zero at the final stage of relaxation. The following 10 ns production MD was carried out unrestrained.

The detail of system minimization and relaxation was as follows. First, the whole system, including Pt-DNA adduct or DNA, water molecules and counter-ions, was minimized for 2000 steps of steepest descent (SD) in constant volume condition with a harmonic potential of 500 kcal/mol $Å^2$ (1 cal = 4.184 J) applied to Pt-DNA or DNA to fix its conformation. Second, the system was heated up from 0 K to 300 K and kept in NVT (constant volume and constant temperature) condition with the harmonic restraints unchanged in a 20 ps relaxation MD. Third, the system was further relaxed in another short 20 ps MD in NPT condition with the same harmonic constraints. Fourth, the system was further minimized for 2000

steps of SD in constant volume condition three times, with a weakening harmonic potential of 500, 50 and 5 kcal/mol $Å^2$ respectively. Fifth, the system was heated up from 10 K to 300 K and kept in NVT condition with the harmonic restraints of 5 kcal/mol $Å^2$ in a 20 ps relaxation MD. Sixth, four rounds of 20 ps relaxation MD were carried out in NPT condition with a further weakening harmonic potential of 5, 1, 0.1 and 0 kcal/mol $Å^2$ respectively. Seventh, the system was heated up from 10 K to 300 K in NVT condition with zero restraints in a 20 ps relaxation MD. Finally, the system was heated up for the very last time from 100 K to 300 K at the beginning of 10 ns production MD.

The above protocol was applied to every MD simulation. Other parameters unmentioned were set to default.

2.2.4 MD simulations and trajectory analysis

Twenty-five 10 ns unrestrained and fully solvated MD simulations were carried out by using SANDER module of AMBER v8.0. Five replicas for each of the five starting structures differed only in the MD initial velocity assigned when the system was heated up for the last time. The atomic coordinates of structures were saved every 1 ps. Both the 5' and 3' terminal base pairs were excluded from analysis because, in a few simulations, the terminal bases were not base-paired and in some extreme cases they were stacked with each other. Therefore only the central ten base pairs 5'-d(CTCAG*G*CCTC)-3' were considered in trajectory analysis and the PTRAJ module of AMBER v8.0 was employed.

2.2.5 Hydrogen bond occupancy

A distance of less than 3.3 Å and an angle of greater than 135 ° between the potential hydrogen bond donor and acceptor were used as the criteria for a hydrogen bond formation. The occupancy of one hydrogen bond was defined as the percentage of frames in which the hydrogen bond existed. The hydrogen bond occupancy of one base pair was defined as the average occupancy of hydrogen bonds existing within this base pair. For example, the hydrogen bond occupancy of normal G·C base pair was the average occupancy of the three standard Watson-Crick hydrogen bonds. However, hydrogen bonds were formed between non-complementary bases in damaged DNA adducts because of the distortion and misalignment of bases. When calculating the hydrogen bond occupancy of base pairs, the occupancy of such a hydrogen bond of at least 5% was necessary for consideration and the occupancy was split evenly between two base

pairs.

2.2.6 Inter-proton distance constraint comparison

A set of inter-proton distance constraints was derived from the NMR data and these constraints were used to compute the NMR solution structures by CNS (Crystallography & NMR System) program([2]). In CNS calculation, a distance violation was defined as one inter-proton distance of resulting structure deviated from the range of corresponding distance constraint by more than 0.5 Å. The same criterion was applied when we tried to evaluate how well our MD simulation structures agreed with the NMR data. In other words, for one inter-proton pair, if the average of trajectory derived distance was beyond its constraints by more than 0.5 Å, a distance violation was reported. In addition, we classified these constraints into several categories based on the locations of two protons. The two protons may be from the same nucleotide, from two nucleotides within the same strand (intrastrand) or from two nucleotides on different strands (interstrand). For one proton, it may be a base proton or a sugar pucker proton. The H1' proton was treated as a base proton because its position is largely independent of sugar pucker. All the other protons of the sugar were considered as sugar pucker protons because their positions were strongly influenced by the sugar pucker conformation. Only the distance constrains of the central four base pairs 5'-d(A5G*6G*7C8)-3' were considered in this study.

2.3 Results

2.3.1 Stability of the MD simulations

In order to determine how long it took for the simulations to reach equilibrium and in turn to decide the range of trajectories used for the following analysis, all-atom mass-weighted root-mean-square deviation (RMSD) referenced to the corresponding NMR structures were calculated over all twenty-five trajectories. Based on the plot of average RMSD over time (Figure 2.1), we concluded that all twenty-five simulations reached equilibrium within 2 ns. Therefore our data were derived from the trajectories from 2 ns to 10 ns (final 8 ns) unless mentioned otherwise. The average RMSD was 2.73 ± 0.53 Å over all ten simulations of CP-DNA, 2.08 ± 0.43 Å over all ten simulations of OX-DNA, and 2.80 ± 0.30 Å over all five simulations of B-DNA. In addition, the curves of OX-DNA simulations were well separated from those of CP-DNA and B-DNA simulations; however, the curves of CP-DNA simulations were interlaced with

those of B-DNA simulations. The curves of all ten CP-DNA simulations were interlaced with one another within the final 8 ns. Thus the simulations actually converged to similar equilibrium structures no matter how different the starting structures and/or MD initial velocity were. Similar trends were observed for OX-DNA and B-DNA simulations.

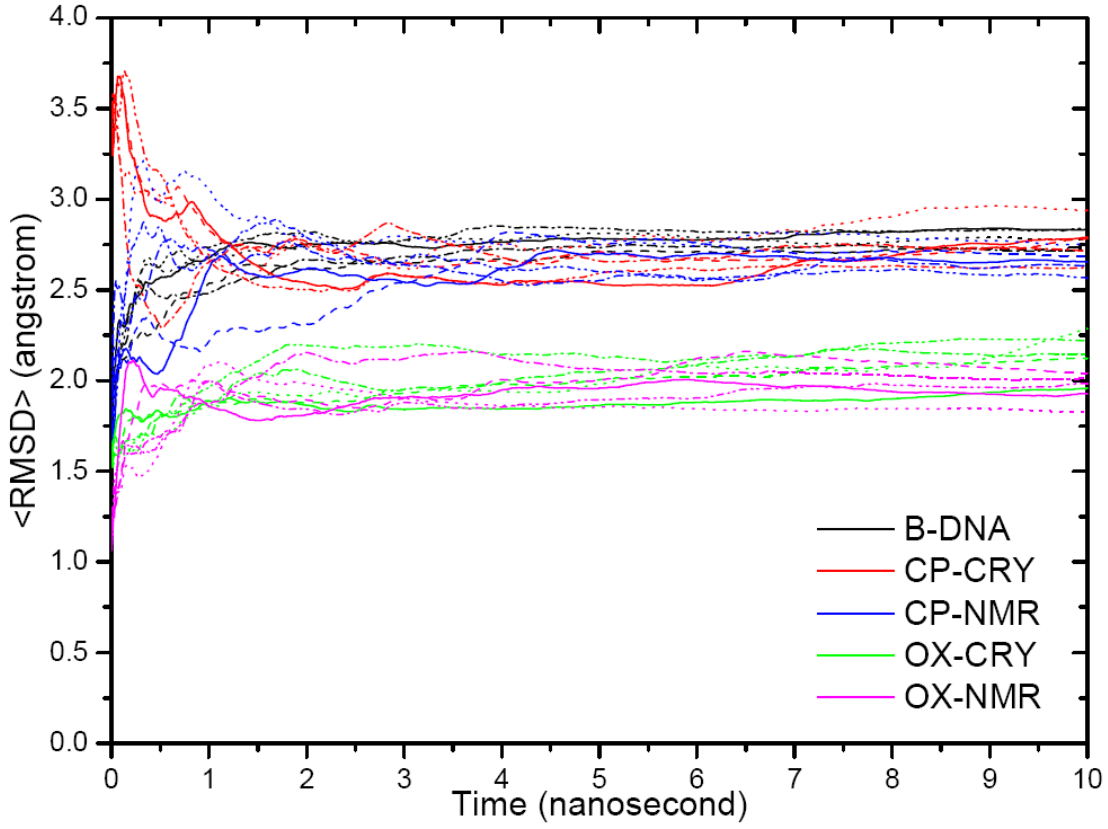

Figure 2.1 The average RMSD over time. <RMSD> at time t stands for the average of RMSD from time zero to time t. B-DNA, CP-NMR and OX-NMR stand for simulations starting from NMR solution structures. CP-CRY and OX-CRY stand for simulations starting from manually built more distorted structures. Five simulation replicas starting from the same structure but with different initial MD velocity are represented in solid line, dash line, dot line, dash-dot line and dash-dot-dot line respectively.

2.3.2 MD simulations reproduced NMR-derived inter-proton distances

In order to assess how well MD simulation structures agreed with corresponding NMR structure, we evaluated to what extent MD simulations reproduced NMR-derived inter-proton distances. There were 171, 160 and 245 inter-proton distance constraints derived from NMR data within the central four base pairs 5'-d(A5G*6G*7C8)-3' of CP-DNA, OX-DNA adducts and B-DNA respectively. The number and detail of distance violations are listed in Tables 2.1 and 2.2 respectively. Most of the violations in CP-DNA simulation structures involved A5 and G*6 nucleotides, which were on the 5' side of the adduct. Overall, there were 5 (< 3%), 2 (< 2%) and 10 (< 5%) violations for CP-DNA, OX-DNA adducts and B-DNA respectively. The very small number of violations compared to the total number of distance constraints

indicated that our MD simulations largely reproduced the NMR data.

		Violations			Total Constraints
		Base-Base Protons	Base-Pucker Protons	Total Violations	
CP-DNA (171)	Inter-Strand	1	0	1	18
	Intra-Strand	1	1	2	43
	Same Nucleotide	0	2	2	110
OX-DNA (160)	Inter-Strand	0	0	0	18
	Intra-Strand	1	1	2	44
	Same Nucleotide	0	0	0	98
B-DNA (245)	Inter-Strand	1	0	1	13
	Intra-Strand	3	3	6	71
	Same Nucleotide	0	3	3	161

Table 2.1 The number of various violations. The very first and last columns give the total number of inter-proton distance constraints and the number of constrains in each category inter-strand, intra-strand and same nucleotide respectively. The middle columns give the number of violations between base and base protons or between base and sugar pucker protons, and the total number of violations in each category.

Cisplatin-DNA				
Proton A	Proton B	NOE Range	NOE Range ± 0.5 Å	Computed NOE
A5H61	T20H3	[2.09, 3.35]	[1.59, 3.85]	3.98 (0.25)
A5H2	G6H1'	[2.75, 4.29]	[2.25, 4.79]	5.10 (0.90)
G6H3'	G7H8	[3.00, 4.70]	[2.50, 5.20]	5.35 (0.91)
A5H8	A5H3'	[2.23, 3.49]	[1.73, 3.99]	4.06 (0.72)
G6H8	G6H3'	[2.34, 3.66]	[1.84, 4.16]	4.26 (0.77)
Oxaliplatin-DNA				
Proton A	Proton B	NOE Range	NOE Range ± 0.5 Å	Computed NOE
A5H2	G6H1'	[3.43, 4.63]	[2.93, 5.13]	5.51 (0.99)
G17H3'	C18H6	[2.92, 3.96]	[2.42, 4.46]	4.60 (0.45)
B-DNA				
Proton A	Proton B	NOE Range	NOE Range ± 0.5 Å	Computed NOE
T20H3	A5H61	[2.01, 3.34]	[1.51, 3.84]	4.00 (0.22)
G17H8	C18H6	[2.67, 4.45]	[2.17, 4.95]	5.05 (0.49)
C8H5	G7H2"	[2.09, 3.48]	[1.59, 3.98]	4.11 (0.56)
A5H1'	G6H4'	[2.92, 4.87]	[2.42, 5.37]	5.39 (0.70)
G7H1'	C8H5	[2.78, 4.63]	[2.28, 5.13]	5.31 (0.49)
C18H5	G17H3'	[3.03, 5.05]	[2.53, 5.55]	5.70 (0.60)
T20H3	C19H42	[2.24, 3.74]	[1.74, 4.24]	4.39 (0.52)
A5H8	A5H2"	[2.10, 3.50]	[1.60, 4.00]	4.18 (0.28)
C18H6	C18H2"	[1.80, 3.00]	[1.30, 3.50]	3.78 (0.29)
C19H5	C19H2"	[3.13, 5.21]	[2.63, 5.71]	5.74 (0.25)

Table 2.2 The detail of violations. The above table lists the detail information about the inter-proton distance violations, showing the two protons involved in the violation, the experimental NOE inter-proton distance constraint range, the NOE range expended outwards by 0.5 Å and the simulation trajectory averaged inter-proton distance with standard deviation in parenthesis.

As a control, we applied the same criterion to the top-15 lowest-energy NMR structures calculated from the CNS program. There were 0 (0%), 0 (0%) and 3 (< 2%) violations for CP-DNA, OX-DNA adducts and B-DNA respectively. The discrepancy in the number of distance violations between our AMBER simulation and CNS calculation were thought to primarily result from the fact that the AMBER simulation was under unrestrained and fully solvated condition, whereas the CNS calculation used the simulated annealing protocol in vacuum and was restrained by the inter-proton distance constraints.

2.3.3 Geometry of the platinum adducts

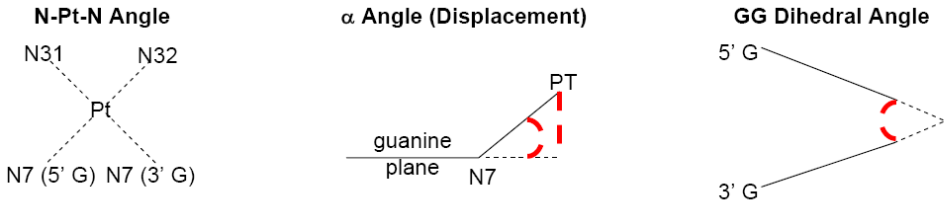

Geometry Parameters	MD Simulated Structures (Final 8 ns)			Top 15 Lowest-Energy NMR Solution Structures		
	CP-DNA	OX-DNA	B-DNA	CP-DNA	OX-DNA	B-DNA
N7(5'G)-Pt-N7(3'G)	88.49 ± 3.24	87.98 ± 3.07	N/A	90.48 ± 0.48	90.40 ± 0.46	N/A
N31-Pt-N32	86.41 ± 4.36	86.19 ± 2.29	N/A	88.77 ± 0.26	85.66 ± 0.06	N/A
N31-Pt-N7(5'G)	92.73 ± 4.02	93.22 ± 3.22	N/A	90.88 ± 0.38	92.00 ± 0.25	N/A
N32-Pt-N7(3'G)	92.19 ± 4.02	92.51 ± 3.22	N/A	89.86 ± 0.32	91.93 ± 0.30	N/A
α angle from 5'G	21.73 ± 7.23	20.96 ± 8.69	N/A	27.30 ± 2.92	40.26 ± 3.83	N/A
α angle from 3'G	14.39 ± 6.20	13.18 ± 5.96	N/A	18.13 ± 1.24	10.04 ± 2.55	N/A
Displacement from 5'G	0.73 ± 0.23	0.70 ± 0.28	N/A	0.92 ± 0.09	1.30 ± 0.10	N/A
Displacement from 3'G	0.49 ± 0.21	0.45 ± 0.20	N/A	0.63 ± 0.04	0.35 ± 0.09	N/A
GG Dihedral Angle	44.31 ± 11.36	44.99 ± 12.56	8.34 ± 4.23	44.89 ± 2.11	35.97 ± 2.65	10.23 ± 4.18

Table 2.3 The platinum geometry. The upper panel illustrates the three kinds of platinum geometry we are interested in, the four N-Pt-N angles (N31 and N32 are two nitrogen atoms from the amine groups of the platinum ligand), the α angle (the angle between Pt-N7 bond and the plane of guanine ring) and displacement (the distance of the platinum atom from the plane of guanine ring), and the GG dihedral angle (the dihedral angle of the two guanine ring planes). The lower table lists the average and standard deviation of each geometry parameter from the 8 ns simulation trajectories and top-15 lowest energy NMR solution structures for cisplatin-DNA, oxaliplatin-DNA adducts and B-DNA respectively.

The geometry parameters (shown and explained in Table 2.3) of platinum adducts derived from both simulation structures and NMR structures are listed in Table 2.3. There are some differences in the geometry of platinum adducts between CP-DNA and OX-DNA adducts based on the data derived from our NMR structures, such as the GG dihedral angle, the α angle and displacement of the platinum atom out of the guanine plane for both 5' and 3' guanines. However, all these differences are diminished in data derived from our simulation structures. For example, the α angles from the 5' G* are 27.30 ± 2.92 º and 40.26 ± 3.83 º for the NMR structures of CP-DNA and OX-DNA adducts respectively; whereas they are 21.73 ± 7.23 º and 20.96 ± 8.69 º for the simulation structures of CP-DNA and OX-DNA adducts respectively, of which the difference of averages is much smaller than the sum of standard deviations.

2.3.4 Hydrogen bonds

In this work, we sought all possible hydrogen bonds through all potential hydrogen bond donors and acceptors, and we calculated the occupancy of all possible hydrogen bonds. We calculated the standard and

non-standard Watson-Crick hydrogen bond occupancy of each base pair for CP-DNA, OX-DNA adducts and B-DNA. The data are plotted in Figure 2.2. When compared to B-DNA, both CP-DNA and OX-DNA adducts show a significant decrease on standard Watson-Crick hydrogen bond occupancy in the 5' G*6·C19 base pair and a considerable decrease in the A5·T20 base pair on the 5' side of the adduct, whereas the base pairs on the 3' side of the adduct are almost completely intact. Meanwhile, a considerable increase on non-standard Watson-Crick hydrogen bond occupancy was found in the 5' G*6·C19 base pair and noticeable increases in the 5' A5·T20 and 3' G*7·C18 base pairs as well, presumably compensating the loss of standard Watson-Crick hydrogen bonds. Two other hydrogen bonds with significantly high occupancy between the platinum carrier ligand and the DNA were identified and are shown in Figure 2.3. One is between the 3' amine hydrogen of the platinum and the oxygen atom O6 of the 3' G*7, with occupancy of 21.4% and 53.5% for CP-DNA and OX-DNA adducts respectively. The other is between the 5' amine hydrogen of the platinum and the nitrogen atom N7 of A5, with occupancy of 61.8% and 34.5% for CP-DNA and OX-DNA adducts respectively. The details of these hydrogen bonds with their occupancies are listed in Table 2.4.

Average Occupancy of Standard Wastson-Crick Hydrogen Bonds of Base Pair (%)			
Base Pair	B-DNA	CP-DNA	OX-DNA
C2-G23	97.58	97.57	97.01
T3-A22	95.52	96.04	96.54
C4-G21	98.56	98.54	98.67
A5-T20	96.31	91.54	92.43
G6-C19	98.32	84.34	86.06
G7-C18	98.46	97.07	96.52
C8-G17	98.75	98.62	98.33
C9-G16	98.05	98.23	98.37
T10-A15	96.00	96.19	95.88
C11-G14	98.53	98.31	98.24
Occupancy of Abnormal Base-Base Hydrogen Bonds (%)			
Donor … Acceptor	B-DNA	CP-DNA	OX-DNA
G6NH1 ... C19O2	2.27	14.26	10.45
G6NH1 ... T20O2	0.00	6.28	6.24
G6NH2 ... T20O2	0.01	5.76	6.41
G7NH1 ... C18O2	2.90	6.89	9.02
Occupancy of Hydrogen Bonds Between Platinum Amine and Base (%)			
Donor … Acceptor	B-DNA	CP-DNA	OX-DNA
Pt25N31 … A5N7	N/A	61.81	34.46
Pt25N32 … G7O6	N/A	21.43	53.48
Pt25N31 … G6O1P	N/A	0.58	0.00

Table 2.4 Hydrogen bond occupancy. The above table gives the detail information of hydrogen bond occupancy in three cases.

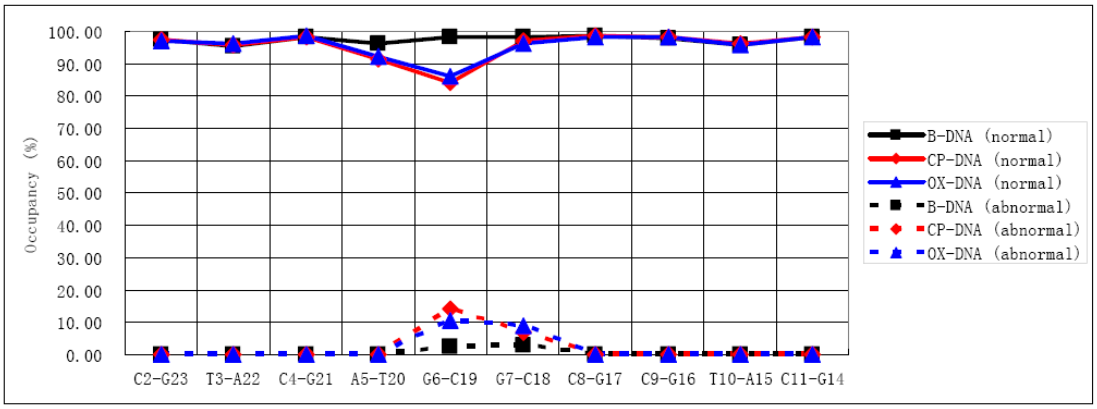

Figure 2.2 Hydrogen bond occupancy of base pairs. The above plot illustrates the significant decreases in the standard Watson-Crick hydrogen bond occupancy and the significant increases in the abnormal hydrogen bond occupancy of base pair at the platinum crosslink lesion. The B-DNA, cisplatin-DNA and

oxaliplatin-DNA are in black, red and blue respectively. The standard Watson-Crick hydrogen bond occupancy of base pair and the abnormal hydrogen bond occupancy of base pair are in solid line and dash line respectively.

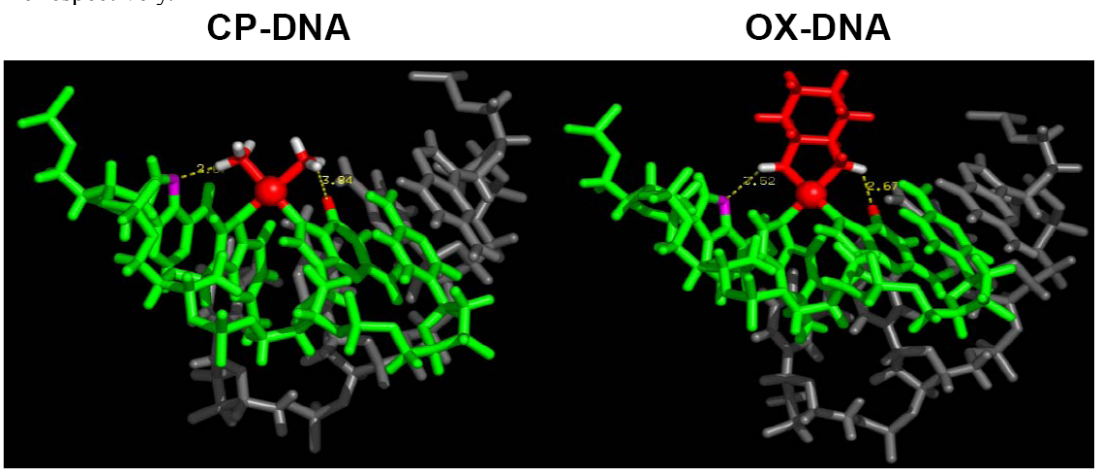

Figure 2.3 Hydrogen bonds between platinum carrier ligand and DNA. Within the DNA which is in green, the pink part represents the N7 atom of A5 and the red part represents the O6 atom of G*7. The platinum adducts are mostly in red. The gray parts of the platinum adducts are the amine hydrogen atoms. The dash lines illustrate the potential hydrogen bonds between the platinum amine groups and the DNA bases.

2.3.5 Torsion angles of the phosphodiester bond connecting the 5' G*6 and 3' G*7

In order to evaluate the flexibility of the phosphodiester bond connecting the 5' G*6 and 3' G*7, we calculated the torsion angles on the 5' side of G*7P (the phosphate atom between G*6 and G*7): G6C2'-G6C3'-G6O3'-G7P, G6C4'-G6C3'-G6O3'-G7P (epsilon, ε) and G6C3'-G6O3'-G7P-G7O5' (zeta, ζ), and on the 3' side of G*7P: G6O3'-G7P-G7O5'-G7C5' (alpha, α), G7P-G7O5'-G7C5'-G7C4' (beta, β), G7O5'-G7C5'-G7C4'-G7C3' (gamma, γ) and G7O5'-G7C5'-G7C4'-G7O4' using the program CURVES v5.3([8]). The frequency distributions of these torsion angles were used for comparison. The frequency distribution measured the probability of torsion angle ranging from -180 ° to +180 °. The frequency distributions of each torsion angle for CP-DNA, OX-DNA adducts and B-DNA are plotted together in red, green and blue respectively in Figure 2.4.

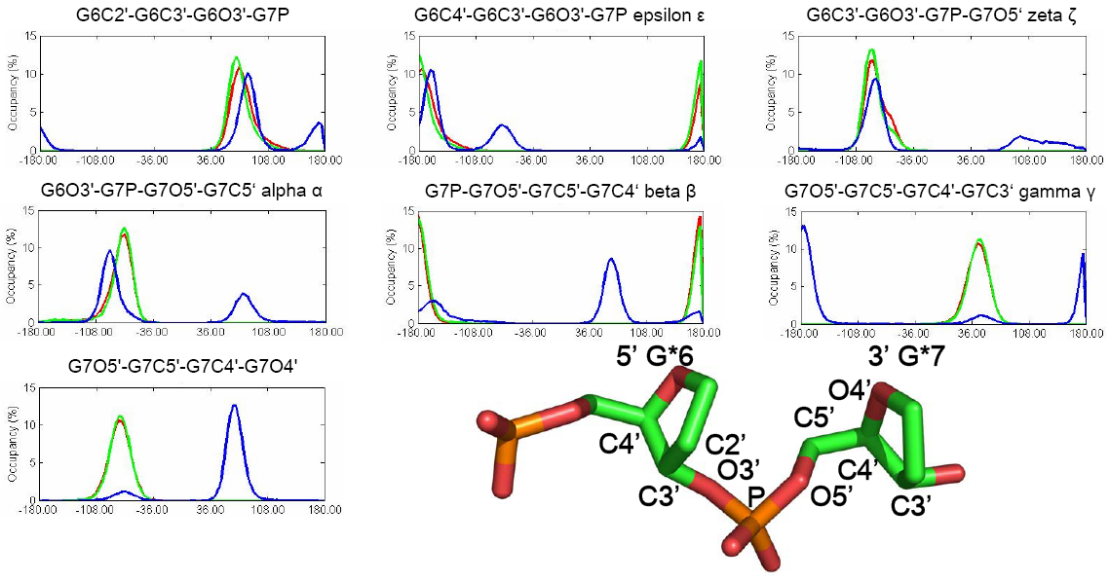

Figure 2.4 The frequency distributions of torsion angles of the phosphodiester bond. In each frequency distribution plot, the B-DNA, cisplatin-DNA and oxaliplatin-DNA are in blue, red and green respectively. The first row of frequency distributions are the three torsion angles from the 3' side of the phosphodiester bond. The rest of the frequency distributions are the four torsion angles from the 5' side of the phosphodiester bond. In the structure illustration, the atoms on the left side of P belong to the 5' G*6 and the atoms on the right side of P including P belong to the 3' G*7.

Overall, for every torsion angle, the frequency distribution of B-DNA had one significant major peak and one much smaller secondary peak. The frequency distributions of CP-DNA and OX-DNA adducts were similar to each other. In addition, the frequency distribution of Pt-DNA adducts had only one major peak and lacked in the secondary peak. For all three torsion angles on the 5' side of G*7P, the major peaks of Pt-DNA adducts were overlapped with the major peak of B-DNA. However, for the three out of four torsion angles on the 3' side of G*7P, the major peaks of Pt-DNA adducts were overlapped with the secondary peak of B-DNA. As compared to B-DNA, in Pt-DNA adducts, the G7O5'-G7C5'-G7C4'-G7O4' torsion angle was shifted from around 72 ° to around -72 °; the γ torsion angle was shifted from around ±180 ° to around 36 °; and the β torsion angle was shifted from around 72 ° to around ±180 °.

2.3.6 DNA conformational dynamics

NMR and x-ray crystallography structures could provide us conformation but not conformational dynamics information, which is an intrinsic advantage of MD simulation. We could monitor the variations of selected parameters in a time-dependent fashion from the MD trajectory. In this work, we assessed the DNA conformational dynamics through the DNA duplex helical parameters because they could provide an accurate description of relative position between two complementary bases and between two adjacent bases

and base pairs. The helical parameters were calculated using the program CURVES v5.3. The frequency distributions of these helical parameters of the central four base pairs of undamaged B-DNA were used for comparison. The frequency distribution illustrated the probability of every conformation cluster explored in MD simulation and it could tell us which conformation was more preferred and which one was not. The frequency distributions of each helical parameter for CP-DNA, OX-DNA adducts and B-DNA are plotted together in red, green and blue respectively in Figures 2.5.

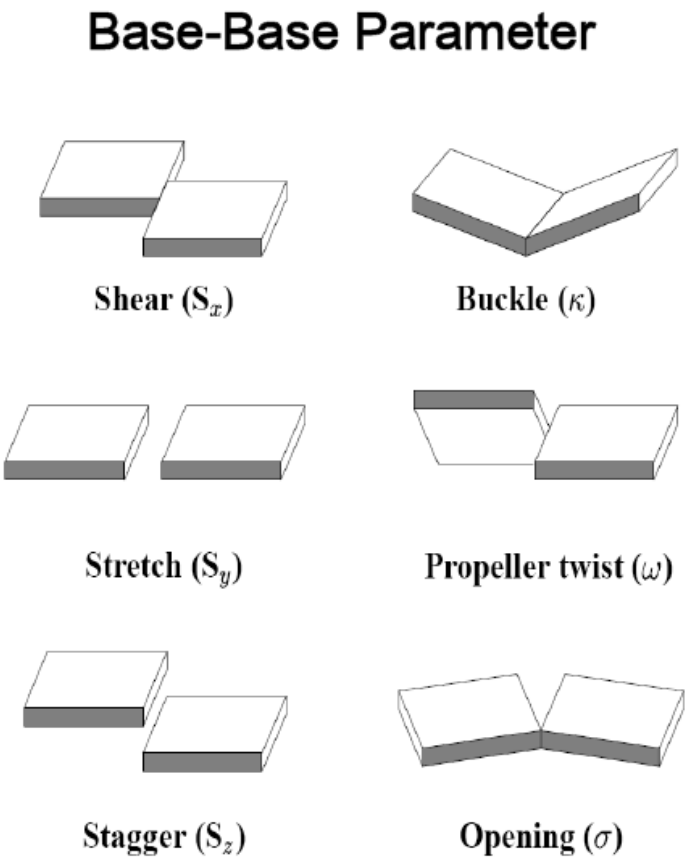

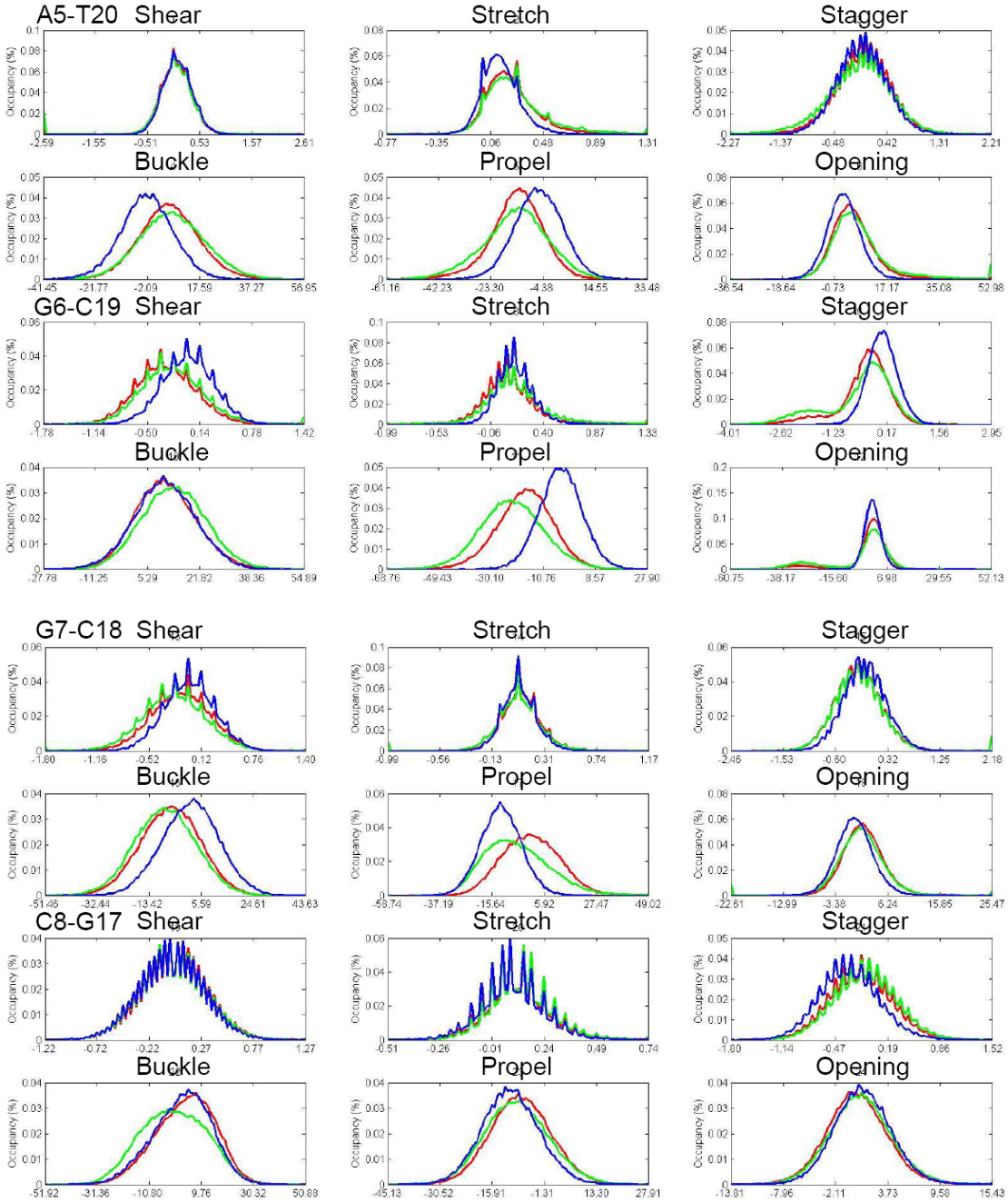
A5-T20 Shear
Stretch
Stagger
Buckle
Propel
Opening
G6-C19 Shear
Stretch
Stagger
Buckle
Propel
Opening
G7-C18 Shear
Stretch
Stagger
Buckle
Propel
Opening
C8-G17 Shear
Stretch
Stagger
Buckle
Propel
Opening
Occupancy (%)

Base-Pair-Step Parameter

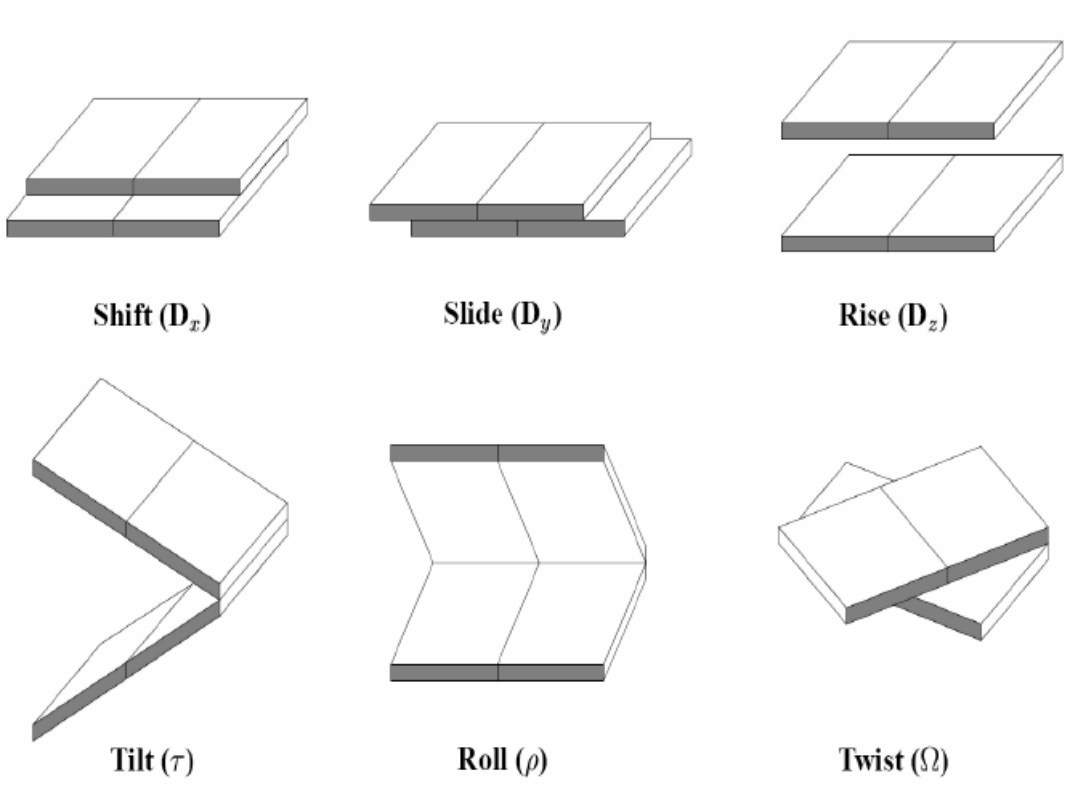

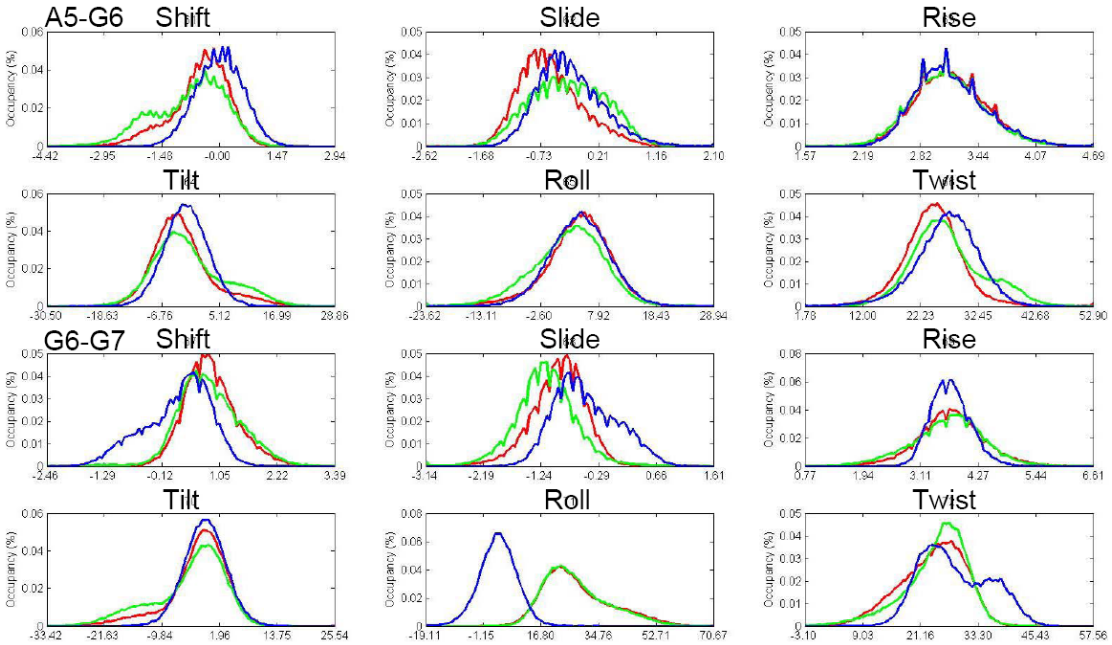

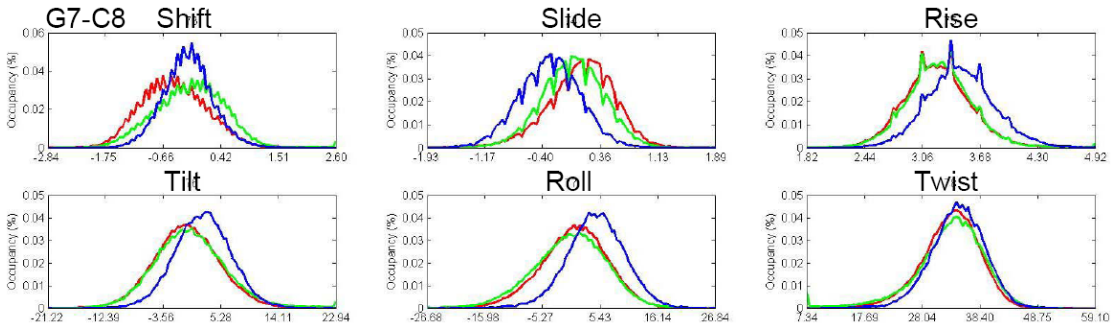

Figure 2.5 The DNA duplex helical parameters for the central four base pairs. The above figures first illustrate what are the base-base and base-pair-step helical parameters and then give the frequency distribution of each parameter for the central four base pairs. In each frequency distribution plot, the B-DNA, cisplatin-DNA and oxaliplatin-DNA are in blue, red and green respectively.

When comparing both Pt-DNA adducts to B-DNA, several striking differences were identified, including buckle and propeller twist for the A5·T20 base pair, shear and propeller twist for the G*6·C19 base pair, buckle and propeller twist for the G*7·C18 base pair; roll at the G*6·C19/G*7·C18 base pair step, and slide, tilt and roll at the G*7·C18/C8·G17 base pair step. These differences indicated that the conformational dynamics profile of B-DNA was alternated by the platinum adducts.

When comparing CP-DNA to OX-DNA, some considerable differences were observed. For base-base helical parameters, noticeable differences were observed for propeller twist for the G*6·C19 and G*7·C18 base pairs and buckle for the C8·G17 base pair. For base-pair-step helical parameters, shift and slide were different at all three base pair steps, particularly slide at the A5·T20/G*6·C19 and G*6·C19/G*7·C18 base pair steps and shift at the G*7·C18/C8·G17 base pair step. At the G*6·C19/G*7·C18 base pair step, the profiles of frequency distribution of roll were almost identical for CP-DNA and OX-DNA adducts, which was consistent with the GG dihedral angles for these two adducts. At the A5·T20/G*6·C19 base pair step, the profiles of frequency distribution of OX-DNA appeared to be relatively more spread out with a heavier tail on one side particularly for shift and twist compared to the CP-DNA adduct, which may imply that the OX-DNA adduct was more flexible between these two base pairs than the CP-DNA adduct. All of the above differences suggest that CP-DNA and OX-DNA differed in conformational dynamics.

2.4 Discussion

2.4.1 Accuracy of MD simulations

We have developed the new partial charge parameters for CP-GG and OX-GG adducts. The new

partial charges on the platinum atom were similar to the previous published value. However, the new partial charges on the surrounding nitrogen atoms were significantly different. Therefore, it was important to validate the accuracy of our new partial charges in MD simulations.

Our MD simulations did reasonably reproduce the NMR solution structures and our simulation structures did share some important geometry characteristics with the NMR solution structures. First, the simulation structures reached equilibrium within 2 ns. The equilibrium structures in the final 8 ns had the average RMSD around 3 Å with respect to the NMR solution structures and they were independent from the starting structures and MD initial velocities. Second, there were less than 5% violations of NMR-derived inter-proton distance constraints and the majority of these violations involved sugar pucker protons. Third, both CP-DNA and OX-DNA adducts in our MD simulations showed significantly increased roll angle at the G*6·C19/G*7·C18 base pair step and the GG dihedral angle with respect to the undamaged B-DNA. The square-planar platinum geometry and the 90 ° of the four N-Pt-N angles were well preserved. These geometry features were consistent with the experimental observations of Pt-DNA adducts.

However, our MD simulations did not reproduce the differences between CP-DNA and OX-DNA adducts in the α angles and displacements of the platinum atom out of the 5’ and 3’ guanine planes, and the GG dihedral angle. The possible reasons were as follows.

First, our new partial charges of CP-GG and OX-GG were similar to each other on the platinum atom and surrounding nitrogen atoms. The rest of the force field parameters and the protocol applied to the MD simulations were identical, which may lead to somewhat similar results from CP-DNA and OX-DNA simulations although their carrier ligands were structurally distinct from each other. However, we did observe quite a few conformation and conformational dynamics differences between CP-DNA and OX-DNA in our MD simulations.

Second, the platinum geometry of our NMR solution structures was not derived directly from our NMR experimental data, but rather determined from CNS calculation. However, there were a few important differences between the CNS calculation and the AMBER MD simulation. The old partial charge parameters of Pt-GG were used in the CNS calculation whereas the AMBER simulation employed the new

parameters. The simulated annealing protocol used in the CNS calculation was in vacuum and restrained by NMR data, while the AMBER simulation was in fully solvated condition and unrestrained. What impacts these differences have on the final resulting structures are currently under investigation.

2.4.2 The DNA duplex is more distorted on the 5' side of the adduct than on the 3' side

Several authors have reported that the majority of the misinsertion mutations occurred opposite the 5'G([1]). In previous work, we have shown that DNA polymerase η and β both catalyzed translesion synthesis with higher efficiency in insertion of a dNTP opposite the 5' G* than opposite the 3'G*([1,3]). Marzilli and co-workers have illustrated a faster exchange rate between the water and imino proton of 5' G*, and furthermore, an unusually large positive shift and slide at 5' X/G* base pair step([10]). Elizondo-Riojas and Kozelka, in their MD simulations, have shown greater mobility of 5' G*·C base pair([4]). All of these previous studies have indicated that the 5' G*·C base pair was more flexible and more distorted than the 3' G*·C base pair. In this work, we provide further evidences from our MD simulations to support this idea.

First, there were more inter-proton distance violations found involving 5' G*6·C19 base pair than involving 3' G*7·C18 base pair, which may imply the abnormality of 5' G*6·C19 base pair. Secondly most convincingly, there was a significantly greater decrease of occupancy of standard Watson-Crick hydrogen bonds within the 5' G*6·C19 base pair than the 3' G*7·C18 base pair.

The DNA sequence context may play a role here since we had the two platinated G*·C base pairs sandwiched by different base pairs, A·T base pair on the 5' side and C·G base pair on the 3' side. The reason we chose this asymmetric "AG*G*C" sequence context was that "AGG" appeared to be the most mutagenic sequence context, and in addition, all of our previous experimental studies employed the DNA template in the "AG*G*C" sequence context. However, most structural and experimental evidences supporting the idea that the 5' G*·C base pair was more distorted than the 3' G*·C base pair were from DNA templates in symmetric sequence contexts.

Although the two nucleotides coordinated to the platinum adduct were guanines and the geometry of Pt-GG appeared to be symmetric, the phosphodiester bond connecting the two guanines was in asymmetric geometry with respect to the phosphate atom. Therefore we hypothesized that the phosphodiester bond may

provide an explanation to the asymmetric distortion of Pt-DNA adducts. Currently we checked the torsion angles of the phosphodiester bond connecting 5' G*6 and 3' G*7. Since we had the MD simulations of undamaged B-DNA in the same sequence context with Pt-DNA adducts, we had a complete set of data for comparison between damaged and undamaged DNA, and between CP-DNA and OX-DNA adducts. In addition, as far as we know, this is the first attempt to correlate the phosphodiester bond with the asymmetric distortion of Pt-DNA adducts.

From the comparison of frequency distribution of torsion angle, our most significant observation was that the three torsion angles in Pt-DNA adducts on the 3' side of the phosphodiester bond between G*6 and G*7 were significantly different from those in B-DNA. These torsion angles in Pt-DNA adducts physically existed but were not preferred in undamaged B-DNA, while the torsion angles on the 5' side of the phosphodiester bond in Pt-DNA adducts were similar to the predominant torsion angles in undamaged B-DNA. The significant torsion angle differences between Pt-DNA adducts and undamaged B-DNA on the 3' side of the phosphodiester bond may indicate that the 3' side of the phosphodiester bond was more flexible than the 5' side. Since the two coordinating guanines had to adapt an altered conformation to accommodate the conformational constraints imposed by the platinum adducts, the different flexibility of the phosphodiester bond on the 5' side and 3' side with respect to the phosphate may result in the distortion of the two guanines to a different extent. The more rigid 5' side of the phosphodiester bond may cause the 5' G*6 to adapt a more severe distortion whereas the more flexible 3' side of the phosphodiester bond may share part of the conformational constraints imposed on the 3' G*7, resulting in less distortion of the 3' G*7. Our data showed that the three torsion angles on the 3' side of the phosphodiester bond were in unfavorable conformations for undamaged B-DNA, whereas the 3' G*7 more or less was in a normal conformation, supporting the idea above. In addition, for all seven torsion angles, the frequency distributions for Pt-DNA adducts lacked the minor conformations observed for undamaged B-DNA, which may suggest that Pt-DNA adducts reduced the flexibility of the phosphodiester backbone on both sides.

In order to further test our hypothesis that the more distorted base pairs on the 5' side of the adduct may result from the flexibility of the phosphodiester bond, we plan to check the torsion angles of the rest of the phosphodiester bonds within the central four base pairs and the work is in progress.

In addition, from our MD simulations, most inter-proton distance violations involved the A5·T20 base pair and there was considerable decrease of occupancy of normal Watson-Crick hydrogen bonds within the A5·T20 base pair. The above two evidences were consistent with the experimental observation that extension from the Pt-DNA adduct was also strongly inhibited([11]).

2.4.3 Conformational differences between CP-DNA and OX-DNA adducts

It has been reported that in the crystal structure of CP-DNA adduct, there was one hydrogen bond formed between the hydrogen atom of one of the two ammine NH_3 ligands and a terminal oxygen atom of the 5' G* 5' phosphate group; and in the crystal structure of OX-DNA adduct, there was one hydrogen bond formed between the pseudo-equatorial hydrogen atom of the amine NH_2 group of the DACH ligand *cis* to the 3' G* and the oxygen atom O6 of the 3' G* (N-O distance 2.9 Å; N-H···O angle 136 °). Thus it has been suggested that the *cis*-diammine carrier ligand of cisplatin was oriented more towards the 5' side of the adduct and the (*trans*-R,R)1,2-diaminocyclohexane DACH carrier ligand of oxaliplatin was oriented more towards the 3' side of the adduct.

However, both hydrogen bonds have not been observed in NMR solution structures of either CP-DNA or OX-DNA adducts. Although our NMR data of OX-DNA adduct showed that the DACH ring was asymmetrically oriented, given the lack of downfield chemical shifts and broad line widths for the amino protons associated with DACH, we concluded that there was no hydrogen bond between the DACH ligand and DNA in our NMR solution structure of the OX-DNA adduct([19]). But some have suggested that there might be hydrogen bond between the NH_3 ligand and the O6 atom of the 3'G* in CP-DNA adduct([20]).

In this study, we did check the occupancy of these two hydrogen bonds for both CP-DNA and OX-DNA adducts. We found that the occupancy of the hydrogen bond reported in the crystal structure of CP-DNA adduct was less than 1% for both CP-DNA and OX-DNA adducts. Our data suggest that the formation of such a hydrogen bond is a rare event, and the crystal structure of CP-DNA adduct happened to capture this rare conformation, possibly due to crystal packing. In their work based on MD simulations of CP-DNA adduct, Elizondo-Riojas and Kozelka also reported that the formation of this hydrogen bond is a very rare event, unless one considers the possibility of hydrogen bonds bridged by one or two water molecules([4]).

In this work, we did observe significant occupancy of the hydrogen bond formed between the hydrogen atom of the 3' ammine NH_3 ligand of CP or the 3' amine NH_2 group of DACH ligand of OX and the oxygen atom O6 in the purine base of the 3' G*7, which had been previously reported in the crystal structure of OX-DNA adduct, but not CP-DNA adduct. The occupancy of this hydrogen bond was higher for OX-DNA adduct (53.5%) than CP-DNA adduct (21.4%). There was another significant hydrogen bond identified between the hydrogen atom of the 5' ammine NH_3 ligand of CP or the 5' amine NH_2 group of DACH ligand of OX *cis* to the 5' G*6 and the nitrogen atom N7 in the purine base of A5. The occupancy of this hydrogen bond was higher for CP-DNA adduct (61.8%) than OX-DNA adduct (34.5%). It is interesting to note that the latter hydrogen bond was found on the 5' side of the adduct and between 5' NH_3 or NH_2 group of ligand and N7 of A on the 5' side of the adduct. An equilvalent hydrogen bond has been reported in MD simulations by Elizondo-Riojas and Kozelka except that the hydrogen bond was on the 3' side of the adduct and between 3' NH_3 ligand of CP-DNA adduct and N7 of A on the 3' side of the adduct([4]). However, the DNA sequence context of their CP adduct was CG*G*A, which was in a reverse order of our AG*G*C, which may imply that the sequence context of Pt-DNA adducts could play a role in the determination of the conformation of Pt-DNA adducts.

The differences in occupancy of hydrogen bonds between the ammine/amine hydrogen atoms of CP/OX and the bases on the 5' and 3' side of the Pt adducts suggest a difference in the orientation of Pt carrier ligands with respect to the DNA between CP-DNA and OX-DNA adducts. The *cis*-diammine carrier ligand of CP appears to be oriented more towards the 5' side of the adduct and the (*trans*-R,R)1,2-diaminocyclohexane carrier ligand of OX appears to be oriented more towards the 3' side of the adduct. Thus although from our MD simulations we did not observe the hydrogen bond reported in the crystal structure of CP-DNA adduct, our data are consistent with the observation reported by Lippard and colleagues with respect to the preferential orientation of carrier ligands of CP-DNA and OX-DNA adducts.

2.4.4 Differences in conformational dynamics between CP-DNA and OX-DNA adducts

From the comparison of frequency distribution of DNA duplex helical parameters, we did observe differences which may reflect the distinct conformational dynamics between CP-DNA and OX-DNA adducts. In addition, in this work we made a comparison with the undamaged B-DNA in the same sequence

context as the Pt-DNA adducts. Thus we could tell how the platinum adducts altered the conformational dynamic profile of B-DNA, such as roll angle at the G*6·C19/G*7·C18 base pair step.

The DNA duplex helical parameters of which frequency distribution profiles were clearly different between CP-DNA and OX-DNA adducts were propeller twist and/or buckle for the central four base pairs, and shift and slide at central three base pair steps, presumably due to the different platinum adducts. The differences in frequency distribution profiles may indicate that in conformational space, for a given period of time, the percentage of time of CP-DNA adducts in one conformation is different from that of OX-DNA adducts in the equivalent conformation. If such conformation is critical for DNA damage-recognition proteins to bind or for DNA polymerases to bypass these adducts, our findings may provide a biological explanation for the differential recognition of CP-DNA and OX-DNA adducts by these proteins. Future NMR and MD studies are planned to further test this hypothesis.

REFERENCES

1. Bassett, E., Vaisman, A., Havener, J. M., Masutani, C., Hanaoka, F., & Chaney, S. G. (2003). Efficiency of extension of mismatched primer termini across from cisplatin and oxaliplatin adducts by human DNA polymerases beta and eta in vitro. *Biochemistry* 42, 14197-14206.

2. Brunger, A. T., Adams, P. D., Clore, G. M., DeLano, W. L., Gros, P., Grosse-Kunstleve, R. W., Jiang, J. S., Kuszewski, J., Nilges, M., Pannu, N. S., Read, R. J., Rice, L. M., Simonson, T., & Warren, G. L. (1998). Crystallography & NMR system: A new software suite for macromolecular structure determination. *Acta Crystallogr. D. Biol. Crystallogr.* 54 (Pt 5), 905-921.

3. Chaney, S. G., Campbell, S. L., Temple, B., Bassett, E., Wu, Y., & Faldu, M. (2004). Protein interactions with platinum-DNA adducts: from structure to function. *J. Inorg. Biochem.* 98, 1551-1559.

4. Elizondo-Riojas, M. A. & Kozelka, J. (2001). Unrestrained 5 ns molecular dynamics simulation of a cisplatin-DNA 1,2-GG adduct provides a rationale for the NMR features and reveals increased conformational flexibility at the platinum binding site. *J. Mol. Biol.* 314, 1227-1243.

5. Fink, D., Nebel, S., Aebi, S., Zheng, H., Cenni, B., Nehme, A., Christen, R. D., & Howell, S. B. (1996). The role of mismatch repair in platinum drug resistance. *Cancer Res.* 56, 4881-4886.

6. Jennerwein, M. M., Eastman, A., & Khokhar, A. R. (1989). Characterization of adducts produced in DNA by isomeric 1,2-diaminocyclohexaneplatinum(II) complexes. *Chem. -Biol. Interact.* 70, 39-49.

7. Kidani, Y. (1989). Oxaliplatin. *Drugs of the Future* 14, 529-532.

8. Lavery, R. & Sklenar, H. (1989). Defining the structure of irregular nucleic acids: conventions and principles. *J. Biomol. Struct. Dyn.* 6, 655-667.

9. Leopold, W. R., Batzinger, R. P., Miller, E. C., Miller, J. A., & Earhardt, R. H. (1981). Mutagenicity, tumorigenicity, and electrophilic reactivity of the stereoisomeric platinum(II) complexes of 1,2-diaminocyclohexane. *Cancer Res.* 41, 4368-4377.

10. Marzilli, L. G., Saad, J. S., Kuklenyik, Z., Keating, K. A., & Xu, Y. (2001). Relationship of solution and protein-bound structures of DNA duplexes with the major intrastrand cross-link lesions formed on cisplatin binding to DNA. *J. Am. Chem. Soc.* 123, 2764-2770.

11. Masutani, C., Kusumoto, R., Iwai, S., & Hanaoka, F. (2000). Mechanisms of accurate translesion synthesis by human DNA polymerase eta. *EMBO Journal* 19, 3100-3109.

12. Murphy, E. C., Zhurkin, V. B., Louis, J. M., Cornilescu, G., & Clore, G. M. (2001). Structural basis for SRY-dependent 46-X,Y sex reversal: modulation of DNA bending by a naturally occurring point mutation. *J. Mol. Biol* 312, 481-499.

13. Page, J. D., Husain, I., Sancar, A., & Chaney, S. G. (1990). Effect of the diaminocyclohexane carrier ligand on platinum adduct formation, repair, and lethality. *Biochemistry* 29, 1016-1024.

14. Scheeff, E. D., Briggs, J. M., & Howell, S. B. (1999). Molecular modeling of the intrastrand guanine-guanine DNA adducts produced by cisplatin and oxaliplatin. *Mol. Pharmacol.* 56, 633-643.

15. Spingler, B., Whittington, D. A., & Lippard, S. J. (2001). 2.4 A crystal structure of an oxaliplatin 1,2-d(GpG) intrastrand cross-link in a DNA dodecamer duplex. *Inorg. Chem.* 40, 5596-5602.

16. Takahara, P. M., Rosenzweig, A. C., Frederick, C. A., & Lippard, S. J. (1995). Crystal structure of double-stranded DNA containing the major adduct of the anticancer drug cisplatin. *Nature* 377, 649-652.

17. Wei, M., Cohen, S. M., Silverman, A. P., & Lippard, S. J. (2001). Effects of spectator ligands on the specific recognition of intrastrand platinum-DNA cross-links by high mobility group box and TATA-binding proteins. *J. Biol. Chem.* 276, 38774-38780.

18. Woynarowski, J. M., Chapman, W. G., Napier, C., Herzig, M. C. S., & Juniewicz, P. (1998). Sequence- and region-specificity of oxaliplatin adducts in naked and cellular DNA. *Molecular. Pharmacology* 54, 770-777.

19. Wu, Y., Pradhan, P., Havener, J., Boysen, G., Swenberg, J. A., Campbell, S. L., & Chaney, S. G. (2004). NMR solution structure of an oxaliplatin 1,2-d(GG) intrastrand cross-link in a DNA dodecamer duplex. *J. Mol. Biol.* 341, 1251-1269.

20. Yang, D., van Bloom, S. S. G. E., Reedijk, J., van Bloom, J. H., & Wang, A. H. J. (1995). Structure and isomerization of an intrastrand cisplatin-cross-linked octamer DNA duplex by NMR analysis. *Biochemistry* 34, 12912-12920.

21. Yao, S., Plastaras, J. P., & Marzilli, L. G. (1994). A molecular mechanics AMBER-type force field for modeling platinum complexes of guanine derivatives. *Inorg. Chem.* 33, 6061-6077.

22. Zdraveski, Z. Z., Mello, J. A., Farinelli, C. K., Essigmann, J. M., & Marinus, M. G. (2002). MutS preferentially recognizes cisplatin- over oxaliplatin-modified DNA. *J. Biol. Chem.* 277, 1255-1260.

23. Zhai, X., Beckmann, H., Jantzen, H.-M., & Essigmann, J. M. (1998). Cisplatin-DNA adducts inhibit ribosomal RNA synthesis by hijacking the transcription factor human upstream binding factor. *Biochemistry* 37, 16307-16315.

CHAPTER 3 GENERAL DISCUSSION AND FUTURE DIRECTION

In Chapter 1, I briefly introduced molecular dynamics simulation and in Chapter 2, I described in detail how we applied molecular dynamics simulation to study the conformation and conformational dynamics of cisplatin-DNA and oxaliplatin-DNA adducts. Data derived from the simulation trajectories showed that DNA duplexes containing either cisplatin or oxaliplatin adducts were more distorted on the 5' side of the adduct than the 3' side possibly due to the different flexibility of the phosphodiester bond on the 5' side and 3' side. Based on the occupancy of hydrogen bonds between platinum ligand and DNA, cisplatin adduct appears to be oriented more towards the 5' side of the adduct and oxaliplatin adduct more towards the 3' side. Several differences were observed in conformational dynamics between cisplatin-DNA and oxaliplatin-DNA adducts from the frequency distributions of DNA duplex helical parameters. The information derived from simulation trajectories will help to clarify the discrepancies among the published experimental structures and to further elucidate the relationship between conformational dynamics differences and differential recognition by cellular DNA regulatory proteins.

3.1 Limitations of experimental structure study

In Table 3.1, I listed all the experimental structures currently deposited in RCSB data bank on line, which are either cisplatin or oxaliplatin intrastrand-GG adducts with double-stranded DNA. Apparently very few experimental structures are available, for example, only two for oxaliplatin-DNA adduct are deposited because it is not easy and could take a year or two to just obtain an acceptable structure. In addition, although these structures share some conformational features, such as the unwinding and bending of the DNA duplex at the lesion, there are significant discrepancies in the degree of unwinding and bending and in a number of important structural details. These discrepancies may appear to result from the different sequence context of DNA. However, the differences in experimental techniques, procedures, conditions and structural refinement methods of the time may be the primary causes. Therefore, fully reproducing previously obtained experimental structure or testing published results by resolving another experimental structure is difficult. However, molecular dynamics simulation has obvious advantages here.

Pt-DNA Adduct	Experimental Method	PDB ID	Release Date	DNA Sequence Context
CP-DNA Adducts	CRY	1AIO	1997.4	5'-d(CCTCTG*G*TCTCC)-3'
		1CKT	1999.6	5'-d(CCTCTCTG*G*ACCTTCC)-3'
	NMR	1AU5	1998.2	5'-d(CCTG*G*TCC)-3'
		1A84	1998.11	5'-d(CCTCTG*G*TCTCC)-3'
		1KSB	2002.1	5'-d(CTCCG*G*CCT)-3'
OX-DNA Adducts	CRY	1IHH	2001.1	5'-d(CCTCTG*G*TCTCC)-3'
	NMR	1PG9	2004.7	5'-d(CCTCAG*G*CCTCC)-3'

Table 3.1 Experimental structures of Pt-DNA adducts. The above table lists all the experimental structures deposited in RCSB data bank on line by Jun 2006 which are either cisplatin (CP) or oxaliplatin (OX) intrastrand-GG adducts with double-stranded DNA. "CRY" stands for x-ray crystallography and "NMR" stands for nuclear magnetic resonance.

3.2 Advantages of molecular dynamics study

After all, molecular dynamics simulation is a series of computer programs. With current computational power, the simulations I described in detail in chapter 2 can finish within two weeks. In addition, the simulation results are always reproducible if running the same programs given the identical parameter settings. We could easily set up a series of simulations covering various conditions along with complete controls, which generally are not affordable by experiment. Therefore I propose to apply molecular dynamics simulation to a more comprehensive study of cisplatin-DNA and oxaliplatin-DNA adducts, aiming at not only comparison study between the two Pt-DNA adducts but also clarification of those discrepancies among the published experimental structures.

3.3 Design of DNA sequence context

The first thing to do is to design the sequence context of DNA duplex. We are still going to focus our study on intrastrand-GG adducts. From the previous studies, the two G*·C base pairs and the base pair immediately adjacent to them on the 5' and 3' side are most affected by the adducts. The rest of the flanking base pairs on both sides are relatively unaffected. Thus the variation of DNA sequence is restricted within the central four base pairs 5'-d(XG*G*Y)-3'. Since the asymmetric distortion of the DNA on the 5' and 3' side of the adduct is one of the discrepancies, we do not want to introduce the factor which may lead to the asymmetric distortion by sandwiching the two G*·C base pairs with different base pairs on the 5' and 3' side. Therefore, the central two G*·C base pairs are going to be symmetrically sandwiched by the identical base pair and the sequence context of the central four base pairs can be 5'-d(AG*G*A)-3',

5’-d(TG*G*T)-3’, 5’-d(CG*G*C)-3’ and 5’-d(GG*G*G)-3’. The sequences of the rest of the flanking base pairs on both sides are also symmetrically designed to be 5’-d(CCTC)-3’ on the 5’ side and 5’-d(CTCC)-3’ on the 3’ side, which are the most commonly used sequence contexts in the published experimental structures. One example of the entire dodecamer sequence will be 5’-d(CCTCAG*G*ACTCC)-3’.

3.4 Molecular dynamics simulation

Once the sequence context of DNA duplex is determined, we are going to build an ideal B-DNA in straight form and coordinate cisplatin or oxaliplatin adducts to the central two G* at N7 atom using molecular modeling program. The reason we do not use experimental structures as a starting point is that there are no experimental structure available for some of our designed DNA sequences. In addition, in these molecular modeling structures, the N7-Pt-N7 angle, GG dihedral angle and some other platinum geometry parameters are expected to deviate from the experimental and theoretical values significantly since the DNA template is in ideal straight form. Thus once again we will challenge our force field parameters to overcome the distortion of starting structure and produce the intrinsic conformational characteristics of Pt-DNA adducts when simulations reach equilibrium. For each of our designed DNA sequence, three starting structures, one cisplatin-DNA adduct, one oxaliplatin-DNA adduct and one undamaged B-DNA as control will be used. As for the simulation protocol, we plan to further refine the minimization and relaxation procedures. The scripts for production runs will be modified when necessary. As for the simulation duration and number of simulation replicas, from our previous experience, the molecular system with similar size using similar simulation protocol reached equilibrium within 2 ns and therefore 5 ns should be long enough. Five or more replicas to provide enough sampling in conformational space may be a better strategy than a long simulation since a simulation may degrade in a long run.

3.5 Simulation trajectory analysis

Our molecular dynamics simulation goal is to study the possibly significant differences in conformation and conformational dynamics between cisplatin-DNA and oxaliplatin-DNA adducts in various sequence contexts, and meanwhile to clarify some discrepancies among the published experimental structures of these adducts. Both conformation and conformational dynamics information can be derived from the simulation trajectory. The trajectory is nothing but a time series of structures. We could derive conformational parameters from any individual frame of the trajectory or the averages of those

conformational parameters from the partial or entire trajectory. Since the frames of the trajectory are in time-dependent order, we could monitor the variations or dynamic changes of those conformational parameters over time, which is so called conformational dynamics. With the enormous amount of conformational dynamics data, various mathematical and statistical methods could be applied to reveal embedded information, such as histogram analysis which could reveal the frequency distribution of conformational species, principal component analysis which could reveal the dominant ones from multiple parameters, and cross-correlation analysis which could reveal the underlying relationships among parameters, etc. From our previous experience, we will have to find methods to be able to quantitatively evaluate and describe the differences.

3.6 Conformational parameters and interactions we are interested in

For every conformational parameter of the structure, we could derive its conformational dynamics counterpart. The conformational parameters we are going to investigate can be roughly divided into the platinum parameters and the DNA parameters.

The platinum parameters are as follows. First the four N-Pt-N angles, the four N-Pt bond lengths and the planarity which evaluates to what extent the platinum atom and four surrounding nitrogen atoms are in the same plane are worth investigating since these parameters govern the square-planar geometry of platinum which should not be violated in any situation. The detail conformation of the diaminocyclohexane ring of the oxaliplatin adduct is worthy of interest as well, such as bond angles, bond lengths, torsion angles, whether or not the ring is in a chair conformation and so on. The GG dihedral angle, the α angle and displacement of the platinum atom out of the guanine plane for both the 5' and 3' guanines, the torsion angle (C8-N7-Pt-*cis*N) from both the 5' and 3' guanines are also in the list. Theoretically, when the cisplatin or oxaliplatin adduct is coordinated with two guanosines, the platinum atom is in an ideal square-planar geometry, the diaminocyclohexane ring of the oxaliplatin adduct is in an ideal chair conformation, the GG dihedral angle is 90 º, and the α angle and displacement are 0 º and 0 Å respectively for both the 5' and 3' guanines etc. However, in our molecular dynamics simulations, the cisplatin-GG and oxaliplatin-GG are in DNA dodecamer duplex. We would expect the platinum square-planar geometry and the chair conformation of the diaminocyclohexane ring of the oxaliplatin adduct to be well preserved and we would predict a significant deviations in the GG dihedral angle, the α angles and displacements, and the torsion angles from

their theoretic values. These deviations describe the distortion of the platinum geometry in DNA duplex.

The DNA parameters basically include all the parameters which could be used to describe the conformation of a DNA duplex. Partial unwinding and significant bending at the Pt-GG crosslinking lesion are well recognized. But to what extent the DNA duplex is unwound and bent and the direction of DNA bend are not consistent among the published experimental structures. Thus they are worth further investigation. There are also some discrepancies in the sugar pucker conformation of the two guanine nucleotides coordinated to the platinum atom, the width and depth of the minor and major groove of the DNA duplex at the lesion. These geometry characteristics may imply that the normal B-like DNA duplex partially transforms to the A-like DNA duplex at the site of the adduct. Thus all key parameters which could be used to distinguish A-like and B-like DNA duplexes are under investigation. The platinum adduct coordinated to the two guanine rings at the major groove side of the DNA duplex, resulting in a head-to-head coordination of the two guanine rings, affects the DNA duplex helical parameters of the two guanine nucleic acid bases, as well as the two G*·C base pairs and immediately adjacent base pairs. Thus the DNA duplex helical parameters are of interest. In our current work described in Chapter 2 we found the asymmetric flexibility of the phosphodiester bond connecting the two guanine deoxynucleosides coordinated to the platinum adduct. We would like to expand our investigation to the rest of phosphodiester bonds within the central four base pairs. The torsion angles of the sugar pucker and glycosyl bond are under investigation too, especially the torsion angle of the glycosyl bond, which describes the relative position between the sugar pucker and the nucleic acid base. In our current work, we have already found that there was significant difference between the frequency distributions of the torsion angle of the glycosyl bond in the 5' and 3' guanine nucleotides (Figure 3.1).

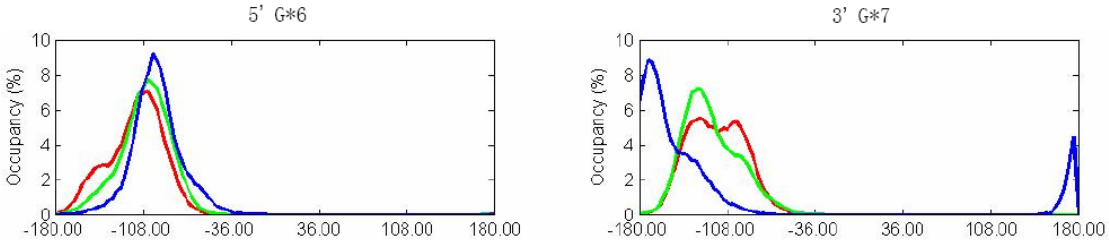

Figure 3.1 The frequency distributions of the torsion angle of the glycosyl bond in the 5' and 3' G*. The B-DNA, cisplatin-DNA and oxaliplatin-DNA are in blue, red and green respectively.

We would also like to characterize all short and long range interactions, including hydrogen bonding, between DNA duplex and platinum adducts, and between solvent molecules and DNA adducts, since these

interactions may be the underlying forces governing the conformation and conformational dynamics.

3.7 Molecular dynamics study on Pt-DNA adducts complex with various DNA regulatory proteins

The next stage of our work is to apply molecular dynamics simulation to study the interactions between Pt-DNA adducts and DNA regulatory proteins, such as HMG-domain proteins and DNA polymerase β. Since the molecular system of Pt-DNA-Protein complex in fully solvated condition may be too big to reach equilibrium within a useful time period, minimization, relaxation and a short production run will be enough to reduce the initial artifacts or unfavorable interactions to an acceptable extent. We will use experimental structures of such Pt-DNA-Protein complexes, if available, as starting structures. We could also rely on molecular modeling, especially when we want to study Pt-DNA-Protein complexes in various DNA sequence contexts. As to molecular modeling, I propose to start from the equilibrium structures of Pt-DNA adducts obtained from previous stage simulations. We could attempt to dock these Pt-DNA adducts to the protein or vice versa based on the experimental evidences of such protein binding with DNA. We will definitely come up more than one Pt-DNA-Protein complex, which will be evaluated with molecular dynamics simulation until we gain faithful structures for further analysis and comparison. Similar conformation and conformational dynamics studies will be applied to the entire molecular system, including the protein. More importantly, we will characterize the significant interactions between the DNA adduct and the protein because these interactions may provide explanations of their biological properties. Based on molecular dynamics simulation results, we are going to generate hypothesizes and test them with biological experiments.

3.8 Future studies

We believe, eventually, molecular dynamics simulation will help us not only to clarify the discrepancies among the published experimental structures, but also to elucidate the biological differences between cisplatin and oxaliplatin adducts with DNA, ultimately contributing to the design of more effective anticancer drugs.

APPENDIX A PT-GG FORCE FIELD PARAMETERS

A.1 PT-GG.prep (for cisplatin-DNA simulation)

```
    1      0      2

db94.dat

modified D-GUANOSINE - with 5' - phosphate group and 3' - O(minus) - N7 replaced by NB1 (atom type
NB replaced by NR)

 DG1   INT        1
 CORR OMIT DU      BEG
   0.0
   1    DUMM   DU      M      0   -1   -2      0.00         0.00         0.00          0.0000
   2    DUMM   DU      M      1    0   -1      1.00         0.00         0.00          0.0000
   3    DUMM   DU      M      2    1    0      1.00        90.00         0.00          0.0000
   4    P      P       M      3    2    1      1.60       119.04       200.00          1.1659
   5    O1P    O2      E      4    3    2      1.48       109.61       150.00         -0.7761
   6    O2P    O2      E      4    3    2      1.48       109.58        20.00         -0.7761
   7    O5'    OS      M      4    3    2      1.60       101.43       -98.89         -0.4954
   8    C5'    CT      M      7    4    3      1.44       119.00       -39.22         -0.0069
   9    H5'1   H1      E      8    7    4      1.09       109.50        60.00          0.0754
  10    H5'2   H1      E      8    7    4      1.09       109.50       -60.00          0.0754
  11    C4'    CT      M      8    7    4      1.52       110.00       180.00          0.1720
  12    H4'    H1      E     11    8    7      1.09       109.50      -200.00          0.1176
  13    O4'    OS      S     11    8    7      1.46       108.86       -86.31         -0.3418
  14    C1'    CT      B     13   11    8      1.42       110.04       105.60          0.1268
  15    H1'    H2      E     14   13   11      1.09       109.50      -240.00          0.2019
  16    N9     N*      S     14   13   11      1.49       108.06      -127.70         -0.4269
  17    C8     CK      B     16   14   13      1.38       129.20        81.59          0.2334
  18    H8     H5      E     17   16   14      1.08       120.00         0.00          0.2173
```

19	NB1	NR	S	17	16	14	1.31	114.00	-179.90	-0.6196
20	C5	CB	S	19	17	16	1.39	103.90	0.00	0.1126
21	C6	C	B	20	19	17	1.42	130.40	180.00	0.5607
22	O6	O	E	21	20	19	1.23	128.80	0.00	-0.4486
23	N1	NA	B	21	20	19	1.40	111.38	180.00	-0.6591
24	H1	H	E	23	21	20	1.00	117.36	179.90	0.3696
25	C2	CA	B	23	21	20	1.38	125.24	-0.10	0.7118
26	N2	N2	B	25	23	21	1.34	116.02	180.00	-0.7661
27	H21	H	E	26	25	23	1.01	127.00	-0.82	0.3853
28	H22	H	E	26	25	23	1.01	116.53	-179.44	0.3853
29	N3	NC	S	25	23	21	1.33	123.30	0.00	-0.4848
30	C4	CB	E	29	25	23	1.36	112.20	0.00	0.4666
31	C3'	CT	M	11	8	7	1.53	115.78	-329.11	0.0804
32	H3'	H1	E	31	11	8	1.09	109.50	30.00	0.0985
33	C2'	CT	B	31	11	8	1.53	102.80	-86.30	-0.0581
34	H2'1	HC	E	33	31	11	1.09	109.50	120.00	0.0809
35	H2'2	HC	E	33	31	11	1.09	109.50	240.00	0.0809
36	O3'	OS	M	31	11	8	1.42	116.52	-203.47	-0.5232

IMPROPER

C8	C4	N9	C1'
C5	N1	C6	O6
C6	C2	N1	H1
C2	H21	N2	H22
NB1	N9	C8	H8
N1	N3	C2	N2

LOOP CLOSING EXPLICIT

C1'	C2'
C4	C5

C4 N9

DONE

modified D-GUANOSINE - with 5' - phosphate group and 3' - O(minus) group - N7 replaced by NB2 (atom type replaced by NS)

DG2 INT 1

CORR OMIT DU BEG

0.0

1	DUMM	DU	M	0	-1	-2	0.00	0.00	0.00	0.0000
2	DUMM	DU	M	1	0	-1	1.00	0.00	0.00	0.0000
3	DUMM	DU	M	2	1	0	1.00	90.00	0.00	0.0000
4	P	P	M	3	2	1	1.60	119.04	200.00	1.1659
5	O1P	O2	E	4	3	2	1.48	109.61	150.00	-0.7761
6	O2P	O2	E	4	3	2	1.48	109.58	20.00	-0.7761
7	O5'	OS	M	4	3	2	1.60	101.43	-98.89	-0.4954
8	C5'	CT	M	7	4	3	1.44	119.00	-39.22	-0.0069
9	H5'1	H1	E	8	7	4	1.09	109.50	60.00	0.0754
10	H5'2	H1	E	8	7	4	1.09	109.50	-60.00	0.0754
11	C4'	CT	M	8	7	4	1.52	110.00	180.00	0.1720
12	H4'	H1	E	11	8	7	1.09	109.50	-200.00	0.1176
13	O4'	OS	S	11	8	7	1.46	108.86	-86.31	-0.3418
14	C1'	CT	B	13	11	8	1.42	110.04	105.60	0.1268
15	H1'	H2	E	14	13	11	1.09	109.50	-240.00	0.2019
16	N9	N*	S	14	13	11	1.49	108.06	-127.70	-0.4269
17	C8	CK	B	16	14	13	1.38	129.20	81.59	0.2334
18	H8	H5	E	17	16	14	1.08	120.00	0.00	0.2173
19	NB2	NS	S	17	16	14	1.31	114.00	-179.90	-0.6196
20	C5	CB	S	19	17	16	1.39	103.90	0.00	0.1126
21	C6	C	B	20	19	17	1.42	130.40	180.00	0.5607

22	O6	O	E	21	20	19	1.23	128.80	0.00	-0.4486
23	N1	NA	B	21	20	19	1.40	111.38	180.00	-0.6591
24	H1	H	E	23	21	20	1.00	117.36	179.90	0.3696
25	C2	CA	B	23	21	20	1.38	125.24	-0.10	0.7118
26	N2	N2	B	25	23	21	1.34	116.02	180.00	-0.7661
27	H21	H	E	26	25	23	1.01	127.00	-0.82	0.3853
28	H22	H	E	26	25	23	1.01	116.53	-179.44	0.3853
29	N3	NC	S	25	23	21	1.33	123.30	0.00	-0.4848
30	C4	CB	E	29	25	23	1.36	112.20	0.00	0.4666
31	C3'	CT	M	11	8	7	1.53	115.78	-329.11	0.0804
32	H3'	H1	E	31	11	8	1.09	109.50	30.00	0.0985
33	C2'	CT	B	31	11	8	1.53	102.80	-86.30	-0.0581
34	H2'1	HC	E	33	31	11	1.09	109.50	120.00	0.0809
35	H2'2	HC	E	33	31	11	1.09	109.50	240.00	0.0809
36	O3'	OS	M	31	11	8	1.42	116.52	-203.47	-0.5232

IMPROPER

C8	C4	N9	C1'
C5	N1	C6	O6
C6	C2	N1	H1
C2	H21	N2	H22
NB2	N9	C8	H8
N1	N3	C2	N2

LOOP CLOSING EXPLICIT

C1'	C2'
C4	C5
C4	N9

DONE

CISPLATIN, (M=Main, S=Side chain dual, B=Side chain trigonal, 3=Side chain tetrahedral, E=End)

```
 PTC    INT         1
 CORR OMIT DU      BEG
    0.0
    1     DUMM    DU       M       0    -1    -2       0.00          0.00          0.00           0.0000
    2     DUMM    DU       M       1     0    -1       1.00          0.00          0.00           0.0000
    3     DUMM    DU       M       2     1     0       1.00         90.00          0.00           0.0000
    4     PT      PT       M       3     2     1       2.01        127.95        180.00           0.7274
    5     N32     N5       3       4     3     2       2.03         90.00        180.00          -0.9656
    6     H321    H        E       5     4     3       1.01        109.47         60.00           0.4224
    7     H322    H        E       5     4     3       1.01        109.47        180.00           0.4224
    8     H323    H        E       5     4     3       1.01        109.47        300.00           0.4224
    9     N31     N4       3       4     3     2       2.03        180.00         70.00          -0.9656
   10     H311    H        E       9     4     3       1.01        109.47         60.00           0.4224
   11     H312    H        E       9     4     3       1.01        109.47        180.00           0.4224
   12     H313    H        E       9     4     3       1.01        109.47        300.00           0.4224
```

DONE

OXALIPLATIN, (M=Main, S=Side chain dual, B=Side chain trigonal, 3=Side chain tetrahedral, E=End)

```
 PTX    INT         1
 CORR OMIT DU      BEG
    0.0
    1     DUMM    DU       M       0    -1    -2       0.00          0.00          0.00           0.0000
    2     DUMM    DU       M       1     0    -1       1.00          0.00          0.00           0.0000
    3     DUMM    DU       M       2     1     0       1.00         90.00          0.00           0.0000
    4     PT      PT       M       3     2     1       2.01        127.95        180.00           0.6889
    5     N32     N5       3       4     3     2       2.03         90.00         90.00          -0.8412
    6     H321    H        E       5     4     3       1.01        109.47         60.00           0.4119
```

7	H322	H	E	5	4	3	1.01	109.47	300.00	0.4119
8	C1	CT	B	5	4	3	1.449	109.47	180.00	0.0273
9	HC11	H1	E	8	5	4	1.090	109.47	-75.23	0.1795
10	C2	CT	3	8	5	4	1.526	109.47	163.78	-0.2881
11	HC21	HC	E	10	8	5	1.090	109.47	300.00	0.1795
12	HC22	HC	E	10	8	5	1.090	109.47	60.00	0.1795
13	C3	CT	3	10	8	5	1.526	109.47	180.00	-0.2881
14	HC31	HC	E	13	10	8	1.090	109.47	300.00	0.1795
15	HC32	HC	E	13	10	8	1.090	109.47	180.00	0.1795
16	C4	CT	3	13	10	8	1.526	109.47	60.00	-0.2881
17	HC41	HC	E	16	13	10	1.090	109.47	60.00	0.1795
18	HC42	HC	E	16	13	10	1.090	109.47	180.00	0.1795
19	C5	CT	3	16	13	10	1.526	109.47	300.00	-0.2881
20	HC51	HC	E	19	16	13	1.090	109.47	180.00	0.1795
21	HC52	HC	E	19	16	13	1.090	109.47	300.00	0.1795
22	C6	CT	S	19	16	13	1.526	109.47	60.00	0.0273
23	HC61	H1	E	22	19	16	1.090	109.47	60.00	0.1795
24	N31	N4	3	4	3	2	2.03	163.45	27.15	-0.8412
25	H311	H	E	24	4	3	1.01	109.47	-71.57	0.4119
26	H312	H	E	24	4	3	1.01	109.47	168.53	0.4119

LOOP CLOSING EXPLICIT

C6 N31

C6 C1

DONE

STOP

Cisplatin-GG				
Guanine (G)	Atom Name	AMBER	OLD	NEW

4	P	1.1659	1.1659	1.1659
5	O1P	-0.7761	-0.7761	-0.7761
6	O2P	-0.7761	-0.7761	-0.7761
7	O5'	-0.4954	-0.4954	-0.4954
8	C5'	-0.0069	-0.0069	-0.0069
9	H5'1	0.0754	0.0754	0.0754
10	H5'2	0.0754	0.0754	0.0754
11	C4'	0.1629	0.1629	0.1720
12	H4'	0.1176	0.1176	0.1176
13	O4'	-0.3691	-0.3691	-0.3418
14	C1'	0.0358	0.0358	0.1268
15	H1'	0.1746	0.1746	0.2019
16	N9	0.0577	0.0807	-0.4269
17	C8	0.0736	0.2466	0.2334
18	H8	0.1997	0.1187	0.2173
19	NB1	-0.5725	-0.3435	-0.6196
20	C5	0.1991	0.2681	0.1126
21	C6	0.4918	0.5148	0.5607
22	O6	-0.5699	-0.5699	-0.4486
23	N1	-0.5053	-0.5053	-0.6591
24	H1	0.3520	0.3520	0.3696
25	C2	0.7432	0.7432	0.7118
26	N2	-0.9230	-0.9230	-0.7661
27	H21	0.4235	0.4235	0.3853
28	H22	0.4235	0.4235	0.3853
29	N3	-0.6636	-0.6636	-0.4848
30	C4	0.1814	0.2044	0.4666
31	C3'	0.0713	0.0713	0.0804
32	H3'	0.0985	0.0985	0.0985
33	C2'	-0.0854	-0.0854	-0.0581
34	H2'1	0.0718	0.0718	0.0809
35	H2'2	0.0718	0.0718	0.0809
36	O3'	-0.5232	-0.5232	-0.5232
Cisplatin	Atom Name		OLD	NEW
4	PT		0.7090	0.7274

5	N32		-0.6480	-0.9656
6	H321		0.2780	0.4224
7	H322		0.2780	0.4224
8	H323		0.2780	0.4224
9	N31		-0.6480	-0.9656
10	H311		0.2780	0.4224
11	H312		0.2780	0.4224
12	H313		0.2780	0.4224
Oxaliplatin-GG				
Guanine (G)	Atom Name	AMBER	OLD	NEW
4	P	1.1659	1.1659	1.1659
5	O1P	-0.7761	-0.7761	-0.7761
6	O2P	-0.7761	-0.7761	-0.7761
7	O5'	-0.4954	-0.4954	-0.4954
8	C5'	-0.0069	-0.0069	-0.0069
9	H5'1	0.0754	0.0754	0.0754
10	H5'2	0.0754	0.0754	0.0754
11	C4'	0.1629	0.1629	0.1717
12	H4'	0.1176	0.1176	0.1176
13	O4'	-0.3691	-0.3691	-0.3427
14	C1'	0.0358	0.0358	0.1238
15	H1'	0.1746	0.1746	0.2010
16	N9	0.0577	0.0807	-0.4283
17	C8	0.0736	0.2466	0.2291
18	H8	0.1997	0.1187	0.2137
19	NB1	-0.5725	-0.3435	-0.5982
20	C5	0.1991	0.2681	0.1122
21	C6	0.4918	0.5148	0.5590
22	O6	-0.5699	-0.5699	-0.4455
23	N1	-0.5053	-0.5053	-0.6599
24	H1	0.3520	0.3520	0.3670
25	C2	0.7432	0.7432	0.7079
26	N2	-0.9230	-0.9230	-0.7649
27	H21	0.4235	0.4235	0.3829
28	H22	0.4235	0.4235	0.3829

29	N3	-0.6636	-0.6636	-0.4856
30	C4	0.1814	0.2044	0.4605
31	C3'	0.0713	0.0713	0.0801
32	H3'	0.0985	0.0985	0.0985
33	C2'	-0.0854	-0.0854	-0.0590
34	H2'1	0.0718	0.0718	0.0806
35	H2'2	0.0718	0.0718	0.0806
36	O3'	-0.5232	-0.5232	-0.5232
Oxaliplatin	Atom Name		OLD	NEW
4	PT		0.7090	0.6889
5	N32		-0.6980	-0.8412
6	H321		0.2780	0.4119
7	H322		0.2780	0.4119
8	C1		0.2620	0.0273
9	HC11		0.0660	0.1795
10	C2		-0.1320	-0.2881
11	HC21		0.0660	0.1795
12	HC22		0.0660	0.1795
13	C3		-0.1320	-0.2881
14	HC31		0.0660	0.1795
15	HC32		0.0660	0.1795
16	C4		-0.1320	-0.2881
17	HC41		0.0660	0.1795
18	HC42		0.0660	0.1795
19	C5		-0.1320	-0.2881
20	HC51		0.0660	0.1795
21	HC52		0.0660	0.1795
22	C6		0.2620	0.0273
23	HC61		0.0660	0.1795
24	N31		-0.6980	-0.8412
25	H311		0.2780	0.4119
26	H312		0.2780	0.4119

Table A.1 Atomic partial charges of CP-GG and OX-GG adducts. The above table lists atomic partial charge of every atom of cisplatin-GG and oxaliplatin-GG adducts. The charges of chemical-equivalent atoms are the same and thus the charges on two guanines are identical. The old charges were developed by Yao *et al.* and Scheeff *et al*. The new charges were developed in this thesis work. The unit of charge is an electron unit (1.602×10^{-19}C)

A.2 frcmod.PT

MASS

PT 195.08 Platinum atom

NR 14.01 0.530 sp2 N N7 of DG1 bound to PT, parm99 values for NB

NS 14.01 0.530 sp2 N N7 of DG2 bound to PT, parm99 values for NB

N4 14.01 0.530 sp3 N PT bound ligand nitrogen, trans to NR, parm99 values for N3

N5 14.01 0.530 sp3 N PT bound ligand nitrogen, trans to NS, parm99 values for N3

BOND

CB-NR 414.0 1.391 JCC,7,(1986),230; ADE,GUA, parm99 values for CB-NB

CB-NS 414.0 1.391 JCC,7,(1986),230; ADE,GUA, parm99 values for CB-NB

CK-NR 529.0 1.304 JCC,7,(1986),230; ADE,GUA, parm99 values for CK-NB

CK-NS 529.0 1.304 JCC,7,(1986),230; ADE,GUA, parm99 values for CK-NB

PT-NR 366.0 2.010 Marzilli InorgChem 33:6061-6067 (1994), Kr = 366 or 183 (183 recommended for duplex DNA)

PT-NS 366.0 2.010 Marzilli InorgChem 33:6061-6067 (1994), Kr = 366 or 183 (183 recommended for duplex DNA)

PT-N4 366.0 2.030 Marzilli InorgChem 33:6061-6067 (1994), Kr = 366 or 183 (183 recommended for duplex DNA)

PT-N5 366.0 2.030 Marzilli InorgChem 33:6061-6067 (1994), Kr = 366 or 183 (183 recommended for duplex DNA)

CT-N4 367.0 1.471 JCC,7,(1986),230; LYS, parm99 values for CT-N3

CT-N5 367.0 1.471 JCC,7,(1986),230; LYS, parm99 values for CT-N3

H -N4 434.0 1.010 JCC,7,(1986),230; LYS, parm99 values for H -N3

H -N5 434.0 1.010 JCC,7,(1986),230; LYS, parm99 values for H -N3

ANGL

C -CB-NR	70.0	130.00	parm99 values for C -CB-NB
CB-CB-NR	70.0	110.40	parm99 values for CB-CB-NB
H5-CK-NR	50.0	123.05	parm99 values for H5-CK-NB
N*-CK-NR	70.0	113.90	parm99 values for N*-CK-NB
CB-NR-CK	70.0	103.80	Scheef MolPharm 56:633-643 (1999), parm99 values for CB-NB-CK
CB-NR-PT	20.0	127.95	Marzilli InorgChem 33:6061-6067 (1994)
CK-NR-PT	20.0	127.95	Marzilli InorgChem 33:6061-6067 (1994)
C -CB-NS	70.0	130.00	parm99 values for C -CB-NB
CB-CB-NS	70.0	110.40	parm99 values for CB-CB-NB
H5-CK-NS	50.0	123.05	parm99 values for H5-CK-NB
N*-CK-NS	70.0	113.90	parm99 values for N*-CK-NB
CB-NS-CK	70.0	103.80	Scheef MolPharm 56:633-643 (1999), parm99 values for CB-NB-CK
CB-NS-PT	20.0	127.95	Marzilli InorgChem 33:6061-6067 (1994)
CK-NS-PT	20.0	127.95	Marzilli InorgChem 33:6061-6067 (1994)
NR-PT-NS	42.0	90.0	Marzilli InorgChem 33:6061-6067 (1994)
N4-PT-N5	42.0	90.0	Marzilli InorgChem 33:6061-6067 (1994)
N4-PT-NS	42.0	90.0	Marzilli InorgChem 33:6061-6067 (1994)
N5-PT-NR	42.0	90.0	Marzilli InorgChem 33:6061-6067 (1994)
N4-PT-NR	42.0	180.0	Marzilli InorgChem 33:6061-6067 (1994)
N5-PT-NS	42.0	180.0	Marzilli InorgChem 33:6061-6067 (1994)
PT-N4-H	50.0	109.5	MODFD Scheef MolPharm 56:633-643 (1999), parm99 values for CT-N3-H
PT-N5-H	50.0	109.5	MODFD Scheef MolPharm 56:633-643 (1999), parm99 values for CT-N3-H
H -N4-H	35.0	109.50	AA lys, AA(end), parm99 values for H -N3-H
H -N5-H	35.0	109.50	AA lys, AA(end), parm99 values for H -N3-H
PT-N4-CT	50.0	109.5	Scheef MolPharm 56:633-643 (1999), parm99 values for

CT-N3-H

PT-N5-CT 50.0 109.5 Scheef MolPharm 56:633-643 (1999), parm99 values for CT-N3-H

CT-N4-H 50.0 109.50 AA lys, changed based on NMA nmodes, parm99 values for CT-N3-H

CT-N5-H 50.0 109.50 AA lys, changed based on NMA nmodes, parm99 values for CT-N3-H

CT-CT-N4 80.0 111.20 AA lys (JCP 76, 1439), parm99 values for CT-CT-N3

CT-CT-N5 80.0 111.20 AA lys (JCP 76, 1439), parm99 values for CT-CT-N3

H1-CT-N4 50.0 109.50 changed based on NMA nmodes, parm99 values for H1-CT-N*

H1-CT-N5 50.0 109.50 changed based on NMA nmodes, parm99 values for H1-CT-N*

DIHE

X -CB-NR-X 2 5.10 180.0 2. parm99, MODFD Scheef MolPharm 56 (1999)

X -CB-NS-X 2 5.10 180.0 2. parm99, MODFD Scheef MolPharm 56 (1999)

X -CK-NR-X 2 20.00 180.0 2. parm99, MODFD Scheef MolPharm 56 (1999)

X -CK-NS-X 2 20.00 180.0 2. parm99, MODFD Scheef MolPharm 56 (1999)

CB-CB-NR-PT 2 0.00 180.0 2. parm99, MODFD Scheef MolPharm 56 (1999)

C -CB-NR-PT 2 0.00 180.0 2. parm99, MODFD Scheef MolPharm 56 (1999)

N*-CK-NR-PT 2 0.00 180.0 2. parm99, MODFD Scheef MolPharm 56 (1999)

H5-CK-NR-PT 2 0.00 180.0 2. parm99, MODFD Scheef

MolPharm 56 (1999)

CB-CB-NS-PT 2 0.00 180.0 2. parm99, MODFD Scheef MolPharm 56 (1999)

C -CB-NS-PT 2 0.00 180.0 2. parm99, MODFD Scheef MolPharm 56 (1999)

N*-CK-NS-PT 2 0.00 180.0 2. parm99, MODFD Scheef MolPharm 56 (1999)

H5-CK-NS-PT 2 0.00 180.0 2. parm99, MODFD Scheef MolPharm 56 (1999)

CB-NR-PT-N5 1 0.50 90.0 2. Marzilli InorgChem 33:6061-6067 (1994)

CK-NR-PT-N5 1 0.50 90.0 2. Marzilli InorgChem 33:6061-6067 (1994)

CB-NR-PT-NS 1 0.50 90.0 2. Marzilli InorgChem 33:6061-6067 (1994)

CK-NR-PT-NS 1 0.50 90.0 2. Marzilli InorgChem 33:6061-6067 (1994)

CB-NR-PT-N4 1 0.00 0.00 2. Scheef MolPharm 56:633-643 (1999)

CK-NR-PT-N4 1 0.00 0.00 2. Scheef MolPharm 56:633-643 (1999)

CB-NS-PT-N4 1 0.50 90.0 2. Marzilli InorgChem 33:6061-6067 (1994)

CK-NS-PT-N4 1 0.50 90.0 2. Marzilli InorgChem 33:6061-6067 (1994)

CB-NS-PT-NR 1 0.50 90.0 2. Marzilli InorgChem 33:6061-6067 (1994)

CK-NS-PT-NR 1 0.50 90.0 2. Marzilli InorgChem 33:6061-6067 (1994)

CB-NS-PT-N5 1 0.00 0.00 2. Scheef MolPharm

56:633-643 (1999)

CK-NS-PT-N5 1 0.00 0.00 2. Scheef MolPharm

56:633-643 (1999)

X -PT-N4-X 9 1.4 0.00 3. Scheef MolPharm 56:633-643

(1999)

X -PT-N5-X 9 1.4 0.00 3. Scheef MolPharm 56:633-643

(1999)

X -CT-N4-X 9 1.40 0.0 3. JCC,7,(1986),230, parm99

values for X -CT-N3-X

X -CT-N5-X 9 1.40 0.0 3. JCC,7,(1986),230, parm99

values for X -CT-N3-X

IMPR

CK-CB-NR-PT 10.0 180. 2. Marzilli InorgChem

33:6061-6067 (1994)

CK-CB-NS-PT 10.0 180. 2. Marzilli InorgChem

33:6061-6067 (1994)

NONB

PT 2.44 0.400 Marzilli InorgChem

33:6061-6067 (1994) diameter ==> radius

NR 1.8240 0.1700 OPLS, parm99

NS 1.8240 0.1700 OPLS, parm99

N4 1.8240 0.1700 OPLS, parm99

N5 1.8240 0.1700 OPLS, parm99

New Atom Type	Mass (1 AMU = 1.66×10^{-27}kg)	Polarizability	Reference		
PT	195.08				
NR	14.01	0.530	1		

NS	14.01	0.530	1		
N4	14.01	0.530	1		
N5	14.01	0.530	1		
Bond	pK (kcal/(mol·Å^2))	Length (Å)	Reference		
CB-NR	414.0	1.391	1		
CB-NS	414.0	1.391	1		
CK-NR	529.0	1.304	1		
CK-NS	529.0	1.304	1		
PT-NR	366.0	2.010	2		
PT-NS	366.0	2.010	2		
PT-N4	366.0	2.030	2		
PT-N5	366.0	2.030	2		
CT-N4	367.0	1.471	1		
CT-N5	367.0	1.471	1		
H-N4	434.0	1.010	1		
H-N5	434.0	1.010	1		
Angle	pK (kcal/(mol·rad^2))	Phase (º)	Reference		
C-CB-NR	70.0	130.00	1		
CB-CB-NR	70.0	110.40	1		
H5-CK-NR	50.0	123.05	1		
N*-CK-NR	70.0	113.90	1		
CB-NR-CK	70.0	103.80	1, 3		
CB-NR-PT	20.0	127.95	2		
CK-NR-PT	20.0	127.95	2		
C-CB-NS	70.0	130.00	1		
CB-CB-NS	70.0	110.40	1		
H5-CK-NS	50.0	123.05	1		
N*-CK-NS	70.0	113.90	1		
CB-NS-CK	70.0	103.80	1, 3		
CB-NS-PT	20.0	127.95	2		
CK-NS-PT	20.0	127.95	2		
NR-PT-NS	42.0	90.00	2		
N4-PT-N5	42.0	90.00	2		
N4-PT-NS	42.0	90.00	2		
N5-PT-NR	42.0	90.00	2		

N4-PT-NR	42.0	180.00	2		
N5-PT-NS	42.0	180.00	2		
PT-N4-H	50.0	109.50	1, 3*		
PT-N5-H	50.0	109.50	1, 3*		
H-N4-H	35.0	109.50	1		
H-N5-H	35.0	109.50	1		
PT-N4-CT	50.0	109.50	1, 3		
PT-N5-CT	50.0	109.50	1, 3		
CT-N4-H	50.0	109.50	1*		
CT-N5-H	50.0	109.50	1*		
CT-CT-N4	80.0	111.20	1		
CT-CT-N5	80.0	111.20	1		
H1-CT-N4	50.0	109.50	1*		
H1-CT-N5	50.0	109.50	1*		
Dihedral Angle	Periodicity	pK (kcal/mol)	Phase (º)	Periodicity	Reference
X-CB-NR-X	2	5.10	180.00	2	1, 3*
X-CB-NS-X	2	5.10	180.00	2	1, 3*
X-CK-NR-X	2	20.00	180.00	2	1, 3*
X-CK-NS-X	2	20.00	180.00	2	1, 3*
CB-CB-NR-PT	2	0.00	180.00	2	1, 3*
C-CB-NR-PT	2	0.00	180.00	2	1, 3*
N*-CK-NR-PT	2	0.00	180.00	2	1, 3*
H5-CK-NR-PT	2	0.00	180.00	2	1, 3*
CB-CB-NS-PT	2	0.00	180.00	2	1, 3*
C-CB-NS-PT	2	0.00	180.00	2	1, 3*
N*-CK-NS-PT	2	0.00	180.00	2	1, 3*
H5-CK-NS-PT	2	0.00	180.00	2	1, 3*
CB-NR-PT-N5	1	0.50	90.00	2	2
CK-NR-PT-N5	1	0.50	90.00	2	2
CB-NR-PT-NS	1	0.50	90.00	2	2
CK-NR-PT-NS	1	0.50	90.00	2	2
CB-NR-PT-N4	1	0.00	0.00	2	3
CK-NR-PT-N4	1	0.00	0.00	2	3
CB-NS-PT-N4	1	0.50	90.00	2	2
CK-NS-PT-N4	1	0.50	90.00	2	2

CB-NS-PT-NR	1	0.50	90.00	2	2
CK-NS-PT-NR	1	0.50	90.00	2	2
CB-NS-PT-N5	1	0.00	0.00	2	3
CK-NS-PT-N5	1	0.00	0.00	2	3
X-PT-N4-X	9	1.40	0.00	3	3
X-PT-N5-X	9	1.40	0.00	3	3
X-CT-N4-X	9	1.40	0.00	3	1
X-CT-N5-X	9	1.40	0.00	3	1
Improper Torsion Angle	pK (kcal/mol)	Phase (º)	Periodicity	Reference	
CK-CB-NR-PT	10	180.00	2	2	
CK-CB-NS-PT	10	180.00	2	2	
Nonbond Interaction	Van der Waals Radius	pK (kcal/mol)	Reference		
PT	2.440	0.40	2		
NR	1.824	0.17	1		
NS	1.824	0.17	1		
N4	1.824	0.17	1		
N5	1.824	0.17	1		

Table A.2 Force field parameters for Pt-GG adducts. AMU stands for atomic mass unit. pK is the penalty constant. The numbers in the reference columns stand for as follows: 1 for parameters from parm99 force field of AMBER, 2 for parameters from work by Yao *et al.* and 3 for parameters from work by Scheeff *et al*. * indicates the parameter is modified based on the original one. The references for Yao *et al.* and Scheeff *et al*. are listed at the end of chapter 2. More detail is presented in the above script file.

APPENDIX B MOLECULAR DYNAMICS SIMULATION PROTOCOL

B.1 LEAP.scr

```
#
#       Read in leaprc
#
source leaprc.ff99
#
#       Set verbosity
#
verbosity 2
#
#               Load atom type hybridizations
#
addAtomTypes {
                { "PT"    "Pt" "sp3" }
                { "NR"    "N"    "sp2" }
                { "NS"    "N"    "sp2" }
                { "N4"    "N"    "sp3" }
                { "N5"    "N"    "sp3" }
}
#
#               Load platinum parameter set.
#
parmPT = loadAmberParams frcmod.PT
#
#               Load platinum libraries
#
loadOff PT.lib
```

```
#
#            Load Generalized Born parameters
#
set default PBradii mbondi
#
#            Load pdb file
#
12mer_cp = loadPdb 12mer_cp.pdb
#
#            Generate new bonds
#
bond 12mer_cp.7.NB1 12mer_cp.25.PT
bond 12mer_cp.6.NB2 12mer_cp.25.PT
#
#            Check unit and parmsets
#
check 12mer_cp parmPT
edit 12mer_cp
```

B.2 SANDER.scr

```
#!/afs/isis/pkg/tcsh/bin/tcsh

cat << eof1 > 12mer_cp_S.min1.in
&cntrl

    IMIN    =            1,
    NTPR    =          100,

    NTB     =            1,
```

```
    CUT     =         9.0,
    NSNB    =          10,

    IGB     =           0,
    NTR     =           1,

    MAXCYC=       2000,
    NCYC    =       5000,

 &end
 Restrain the DNA
 500.0
RES    1    28
END
END
eof1

cat << eof2 > 12mer_cp_S.md2.in
&cntrl

    IMIN    =           0,
    NTX     =           1,
    IREST =             0,
    NTRX    =           1,

    NTPR    =         100,
    NTWX    =           0,

    NTF     =           2,
    NTB     =           1,
```

```
    CUT     =         9.0,
    NSNB    =          10,

    IGB     =           0,
    NTR     =           1,

    NSTLIM=     20000,
    NSCM    =      1000,
    T       =       0.0,
    DT      =     0.001,

    TEMP0 =     300.0,
    TEMPI =       0.0,
    NTT     =           1,
    TAUTP =       0.2,

    NTC     =           2,

 &end
 Restrain the DNA
 500.0
RES   1   28
END
END
eof2

cat << eof3 > 12mer_cp_S.md3.in
&cntrl

    IMIN    =           0,
```

```
  NTX     =     5,
  IREST =     1,
  NTRX    =     1,

  NTPR    =   100,
  NTWX    =     0,

  NTF     =     2,
  NTB     =     2,
  CUT     =   9.0,
  NSNB    =    10,

  IGB     =     0,
  NTR     =     1,

  NSTLIM=  20000,
  NSCM    =  1000,
  T       =   0.0,
  DT      =  0.001,

  TEMP0 =  300.0,
  NTT     =     1,
  TAUTP =   0.2,

  NTP     =     1,
  PRES0 =   1.0,
  TAUP    =   0.2,
  NTC     =     2,

&end
```

```
 Restrain the DNA
 500.0
RES    1    28
END
END
eof3

cat << eof4 > 12mer_cp_S.min4.in
&cntrl

    IMIN    =            1,
    NTPR    =          100,

    NTB     =            1,
    CUT     =          9.0,
    NSNB    =           10,

    IGB     =            0,
    NTR     =            1,

    MAXCYC=         2000,
    NCYC    =        5000,

 &end
 Weaken restraints on DNA
 500.0
RES    1    28
END
END
eof4
```

```
cat << eof5 > 12mer_cp_S.min5.in
&cntrl

    IMIN    =          1,
    NTPR    =        100,

    NTB     =          1,
    CUT     =        9.0,
    NSNB    =         10,

    IGB     =          0,
    NTR     =          1,

    MAXCYC=      2000,
    NCYC    =      5000,

 &end
 Weaken restraints on DNA
 50.0
RES   1   28
END
END
eof5

cat << eof6 > 12mer_cp_S.min6.in
&cntrl

    IMIN    =          1,
    NTPR    =        100,
```

```
    NTB     =           1,
    CUT     =        9.0,
    NSNB    =          10,

    IGB     =           0,
    NTR     =           1,

    MAXCYC=      2000,
    NCYC    =      5000,

  &end
  Weaken restraints on DNA
  5.0
RES    1    28
END
END
eof6

cat << eof7 > 12mer_cp_S.md7.in
&cntrl

    IMIN    =           0,
    NTX     =           1,
    IREST =             0,
    NTRX    =           1,

    NTPR    =         100,
    NTWX    =           0,
```

```
  NTF     =     2,
  NTB     =     1,
  CUT     =   9.0,
  NSNB    =    10,

  IGB     =     0,
  NTR     =     1,

  NSTLIM=  20000,
  NSCM    =  1000,
  T       =   0.0,
  DT      =  0.001,

  TEMP0 =  300.0,
  TEMPI =   10.0,
  NTT     =     1,
  TAUTP =   0.2,

  NTP     =     0,
  PRES0 =   1.0,
  TAUP    =   0.2,
  NTC     =     2,

 &end
 Weaken restraints on DNA
 5.0
RES   1   28
END
END
eof7
```

```
cat << eof8 > 12mer_cp_S.md8.in
&cntrl

    IMIN    =          0,
    NTX     =          5,
    IREST   =          1,
    NTRX    =          1,

    NTPR    =        100,
    NTWX    =          0,

    NTF     =          2,
    NTB     =          2,
    CUT     =        9.0,
    NSNB    =         10,

    IGB     =          0,
    NTR     =          1,

    NSTLIM=    20000,
    NSCM    =     1000,
    T       =      0.0,
    DT      =    0.001,

    TEMP0 =    300.0,
    NTT     =          1,
    TAUTP =      0.2,

    NTP     =          1,
```

```
    PRES0 =         1.0,
    TAUP  =         0.2,
    NTC   =           2,

 &end
 Weaken restraints on DNA
 5.0
RES   1   28
END
END
eof8

cat << eof9 > 12mer_cp_S.md9.in
&cntrl

    IMIN  =           0,
    NTX   =           5,
    IREST =           1,
    NTRX  =           1,

    NTPR  =         100,
    NTWX  =           0,

    NTF   =           2,
    NTB   =           2,
    CUT   =         9.0,
    NSNB  =          10,

    IGB   =           0,
    NTR   =           1,
```

```
    NSTLIM=     20000,
    NSCM   =      1000,
    T      =       0.0,
    DT     =     0.001,

    TEMP0 =     300.0,
    NTT    =         1,
    TAUTP =       0.2,

    NTP    =         1,
    PRES0 =       1.0,
    TAUP   =       0.2,
    NTC    =         2,

 &end
 Weaken restraints on DNA
 1.0
RES   1   28
END
END
eof9

cat << eof10 > 12mer_cp_S.md10.in
&cntrl

    IMIN   =         0,
    NTX    =         5,
    IREST =          1,
    NTRX   =         1,
```

```
  NTPR    =       100,
  NTWX    =         0,

  NTF     =         2,
  NTB     =         2,
  CUT     =       9.0,
  NSNB    =        10,

  IGB     =         0,
  NTR     =         1,

  NSTLIM=    20000,
  NSCM    =     1000,
  T       =      0.0,
  DT      =    0.001,

  TEMP0 =    300.0,
  NTT     =         1,
  TAUTP =      0.2,

  NTP     =         1,
  PRES0 =      1.0,
  TAUP    =      0.2,
  NTC     =         2,

 &end
 Weaken restraints on DNA
 0.1
RES   1   28
```

```
END
END
eof10

cat << eof11 > 12mer_cp_S.md11.in
&cntrl

    IMIN    =     0,
    NTX     =     5,
    IREST   =     1,
    NTRX    =     1,

    NTPR    =   100,
    NTWX    =     0,

    NTF     =     2,
    NTB     =     2,
    CUT     =   9.0,
    NSNB    =    10,

    IGB     =     0,
    NTR     =     0,

    NSTLIM=  20000,
    NSCM    =  1000,
    T       =   0.0,
    DT      =  0.001,

    TEMP0 =  300.0,
    NTT     =     1,
```

```
    TAUTP =         0.2,

    NTP     =           1,
    PRES0 =         1.0,
    TAUP    =         0.2,
    NTC     =           2,

  &end
eof11

cat << eof12 > 12mer_cp_S.md12.in
&cntrl

    IMIN    =           0,
    NTX     =           1,
    IREST =           0,
    NTRX    =           1,

    NTPR    =         100,
    NTWX    =           0,

    NTF     =           2,
    NTB     =           1,
    CUT     =         9.0,
    NSNB    =          10,

    IGB     =           0,
    NTR     =           0,

    NSTLIM=     20000,
```

```
    NSCM    =       1000,
    T       =       0.0,
    DT      =     0.001,

    TEMP0 =     300.0,
    TEMPI =      10.0,
    NTT     =          1,
    TAUTP =       0.2,

    NTC     =          2,

  &end
eof12

cat << eof13 > 12mer_cp_S.md0500.in
&cntrl

    IMIN    =          0,
    NTX     =          1,
    IREST =            0,
    NTRX    =          1,

    NTPR    =        200,
    NTWX    =        200,
    NTWE    =        200,

    NTF     =          2,
    NTB     =          2,
    NTC     =          2,
    CUT     =        9.0,
```

```
    NSNB   =          10,

    IGB    =           0,
    NTR    =           0,

    NSTLIM=   500000,
    NSCM   =      1000,
    T      =       0.0,
    DT     =     0.001,

    TEMPI =     100.0,
    TEMP0 =     300.0,
    NTT    =           1,
    TAUTP =       1.0,
    IG     =     71277,

    NTP    =           1,
    PRES0 =       1.0,
    TAUP   =       2.0,

 &end
eof13

cat << eof14 > 12mer_cp_S.md1000.in
&cntrl

    IMIN   =           0,
    NTX    =           5,
    IREST =           1,
    NTRX   =           1,
```

```
  NTPR    =       200,
  NTWX    =       200,
  NTWE    =       200,

  NTF     =         2,
  NTB     =         2,
  NTC     =         2,
  CUT     =       9.0,
  NSNB    =        10,

  IGB     =         0,
  NTR     =         0,

  NSTLIM=   500000,
  NSCM    =      1000,
  DT      =     0.001,

  TEMP0 =     300.0,
  NTT     =         1,
  TAUTP =       1.0,

  NTP     =         1,
  PRES0 =       1.0,
  TAUP    =       2.0,

 &end
eof14
```

```
mpirun -np 4 /afs/isis/pkg/amber-8/build/amber8/exe/sander -p      12mer_cp_S.top          \
                    -c      12mer_cp_S.crd          \
                    -ref 12mer_cp_S.crd             \
                    -i      12mer_cp_S.min1.in      \
                    -inf 12mer_cp_S.min1.inf    \
                    -o      12mer_cp_S.min1.out     \
                    -r      12mer_cp_S.min1.rstrt

mpirun -np 4 /afs/isis/pkg/amber-8/build/amber8/exe/sander -p      12mer_cp_S.top          \
                    -c      12mer_cp_S.min1.rstrt \
                    -ref 12mer_cp_S.min1.rstrt \
                    -i      12mer_cp_S.md2.in       \
                    -inf 12mer_cp_S.md2.inf     \
                    -o      12mer_cp_S.md2.out      \
                    -r      12mer_cp_S.md2.rstrt

mpirun -np 4 /afs/isis/pkg/amber-8/build/amber8/exe/sander -p      12mer_cp_S.top          \
                    -c      12mer_cp_S.md2.rstrt    \
                    -ref 12mer_cp_S.md2.rstrt   \
                    -i      12mer_cp_S.md3.in       \
                    -inf 12mer_cp_S.md3.inf     \
                    -o      12mer_cp_S.md3.out      \
                    -r      12mer_cp_S.md3.rstrt

mpirun -np 4 /afs/isis/pkg/amber-8/build/amber8/exe/sander -p      12mer_cp_S.top          \
                    -c      12mer_cp_S.md3.rstrt    \
                    -ref 12mer_cp_S.md3.rstrt   \
                    -i      12mer_cp_S.min4.in      \
                    -inf 12mer_cp_S.min4.inf    \
                    -o      12mer_cp_S.min4.out     \
```

```
                -r      12mer_cp_S.min4.rstrt


mpirun -np 4 /afs/isis/pkg/amber-8/build/amber8/exe/sander -p      12mer_cp_S.top          \
                -c      12mer_cp_S.min4.rstrt \
                -ref 12mer_cp_S.min4.rstrt \
                -i      12mer_cp_S.min5.in      \
                -inf 12mer_cp_S.min5.inf    \
                -o      12mer_cp_S.min5.out     \
                -r      12mer_cp_S.min5.rstrt


mpirun -np 4 /afs/isis/pkg/amber-8/build/amber8/exe/sander -p      12mer_cp_S.top          \
                -c      12mer_cp_S.min5.rstrt \
                -ref 12mer_cp_S.min5.rstrt \
                -i      12mer_cp_S.min6.in      \
                -inf 12mer_cp_S.min6.inf    \
                -o      12mer_cp_S.min6.out     \
                -r      12mer_cp_S.min6.rstrt


mpirun -np 4 /afs/isis/pkg/amber-8/build/amber8/exe/sander -p      12mer_cp_S.top          \
                -c      12mer_cp_S.min6.rstrt \
                -ref 12mer_cp_S.min6.rstrt \
                -i      12mer_cp_S.md7.in       \
                -inf 12mer_cp_S.md7.inf     \
                -o      12mer_cp_S.md7.out      \
                -r      12mer_cp_S.md7.rstrt


mpirun -np 4 /afs/isis/pkg/amber-8/build/amber8/exe/sander -p      12mer_cp_S.top          \
                -c      12mer_cp_S.md7.rstrt    \
                -ref 12mer_cp_S.md7.rstrt   \
                -i      12mer_cp_S.md8.in       \
```

```
                -inf 12mer_cp_S.md8.inf       \
                -o   12mer_cp_S.md8.out       \
                -r   12mer_cp_S.md8.rstrt

mpirun -np 4 /afs/isis/pkg/amber-8/build/amber8/exe/sander -p   12mer_cp_S.top          \
                -c   12mer_cp_S.md8.rstrt   \
                -ref 12mer_cp_S.md8.rstrt   \
                -i   12mer_cp_S.md9.in        \
                -inf 12mer_cp_S.md9.inf       \
                -o   12mer_cp_S.md9.out       \
                -r   12mer_cp_S.md9.rstrt

mpirun -np 4 /afs/isis/pkg/amber-8/build/amber8/exe/sander -p   12mer_cp_S.top          \
                -c   12mer_cp_S.md9.rstrt   \
                -ref 12mer_cp_S.md9.rstrt   \
                -i   12mer_cp_S.md10.in       \
                -inf 12mer_cp_S.md10.inf      \
                -o   12mer_cp_S.md10.out      \
                -r   12mer_cp_S.md10.rstrt

mpirun -np 4 /afs/isis/pkg/amber-8/build/amber8/exe/sander -p   12mer_cp_S.top          \
                -c   12mer_cp_S.md10.rstrt \
                -i   12mer_cp_S.md11.in       \
                -inf 12mer_cp_S.md11.inf      \
                -o   12mer_cp_S.md11.out      \
                -r   12mer_cp_S.md11.rstrt

mpirun -np 4 /afs/isis/pkg/amber-8/build/amber8/exe/sander -p   12mer_cp_S.top          \
                -c   12mer_cp_S.md11.rstrt \
                -i   12mer_cp_S.md12.in       \
```

```
                    -inf 12mer_cp_S.md12.inf     \
                    -o     12mer_cp_S.md12.out     \
                    -r     12mer_cp_S.md12.rstrt

mpirun -np 4 /opt/amber/exe/sander -p     12mer_cp_S.top                \
                    -c     12mer_cp_S.md12.rstrt     \
                    -i     12mer_cp_S.md0500.in       \
                    -inf 12mer_cp_S.md0500.inf     \
                    -o     12mer_cp_S.md0500.out     \
                    -x     12mer_cp_S.md0500.mdcrd \
                    -e     12mer_cp_S.md0500.mden    \
                    -r     12mer_cp_S.md0500.rstrt

mpirun -np 4 /opt/amber/exe/sander -p     12mer_cp_S.top                \
                    -c     12mer_cp_S.md0500.rstrt \
                    -i     12mer_cp_S.md1000.in       \
                    -inf 12mer_cp_S.md1000.inf     \
                    -o     12mer_cp_S.md1000.out     \
                    -x     12mer_cp_S.md1000.mdcrd \
                    -e     12mer_cp_S.md1000.mden    \
                    -r     12mer_cp_S.md1000.rstrt
```